Spatial patterns of precipitation-induced moisture availability and their effects on the divergence of tree growth in the western and eastern parts of China's semi-arid region

Xiaomin ZENG [1], Michael N. EVANS [2], Xiaohong LIU [1,3*], Wenzhi WANG [4,5], Guobao XU [3,6], Guoju WU [3], Lingnan ZHANG [1]

1. School of Geography and Tourism, Shaanxi Normal University, Xi'an 710119, China;
2. Department of Geology and Earth System Science Interdisciplinary Center, University of Maryland, College Park, MD, USA;
3. State Key Laboratory of Cryospheric Sciences, Northwest Institute of Eco-Environment and Resources, Chinese Academy of Sciences, Lanzhou 730000, China;
4. Key Laboratory of Mountain Surface Processes and Ecological Regulation, Institute of Mountain Hazards and Environment, Chinese Academy of Sciences, Chengdu 610041, China;
5. Pacific Northwest National Laboratory, Richland, 99352, USA;
6. Laboratory of Tree-Ring Research, University of Arizona, Tucson, 85721, USA;

Running title: Divergence of tree growth in semi-arid China

* Author for Correspondence: Xiaohong Liu

E-mail: xhliu@snnu.edu.cn

Tel.: +86 138-9337-8787

School of Geography and Tourism, Shaanxi Normal University

Chang'an West Road 620, Xi'an, Shaanxi 710119, China

Abstract

Forests in semi-arid regions are fragile and sensitive to climate change. As the climate changes, drought and higher temperatures may reduce tree growth in these regions, but moistening and lengthening of the growing season may improve conditions. The relative influences of specific climate parameters on tree growth however, remain poorly quantified in Asian regions. We analyzed the growth responses to climate in the semi-arid region of China. Our analyses show a wetting trend since 1960 in the western part of this region, versus a drying trend in the east. We used tree-ring width data from a network of 33 forests as inputs for the process-based Vaganov–Shashkin-Lite growth model to assess how moisture patterns have affected tree growth in this region, and then used the resulting model to predict changes in tree growth during the 21st century. Tree-ring growth in our study region is mainly controlled by precipitation and soil moisture, and shows significant impacts of antecedent moisture conditions (the "water memory effect"). However, the contribution of soil moisture to tree growth was stronger in the eastern vs. western sub-regions (77% vs. 69%). Pointer-year analysis showed significantly stronger growth responses to soil moisture in the early growing season (April to June) in positive pointer years in the eastern sub-region, but showed no difference in the western sub-region. These results indicate that tree-ring growth in the eastern sub-region is more vulnerable to moisture availability. Our simulations suggest that tree growth will increase slightly under the RCP 4.5 and RCP 8.5 scenarios in both

sub-regions, possibly due to the prolongation of the growing season caused by climate warming.

Keywords: Drought, semi-arid, tree rings, Vaganov–Shashkin-Lite model, emission scenarios, water memory effect

1. Introduction

Forests play a key role in carbon and water cycles, and influence climate forcing and feedbacks worldwide (Allen et al., 2010; Anderegg et al., 2015; Hagedorn et al., 2016; Peng et al., 2011; Williams et al., 2010). The long-term global warming trend is particularly strong in semi-arid regions (Huang et al., 2012). Both observations and modeling studies indicate that in a warmer climate, droughts may become longer and more severe in currently drought-prone regions because of increased evaporation and reduced precipitation (Dai, 2013; Huang et al., 2015a, 2015b). Among all vegetation types, forests are potentially the most susceptible to drought based on the hydraulic connection between the soil and the atmosphere through vascular plants (McDowell and Allen, 2015). Therefore, learning how tree growth in semi-arid forests will respond to global climate change is crucial to understand how perennial vegetation will adapt to changes in local and even global climate dynamics.

In drought-prone areas, warming-induced increases in the atmospheric moisture demand and decreases in the soil water availability have been widely documented to decrease tree stem radial growth, leading to decline and increased mortality (Allen et al., 2010; Hagedorn et al., 2016; Liang et al., 2016; Liu et al., 2013; McDowell et al.,

2008, 2015; Peng et al., 2011; Williams et al., 2013; Wu et al., 2013, 2018; Xu et al., 2017). Most research focused on warming-induced drought, known as "global-change-type" drought (Breshears et al., 2005), but paid less attention to the other key aspect of drought, namely the water supply (Liu et al., 2018). In arid and semi-arid regions, precipitation-dependent soil moisture is the most direct factor that controls tree growth (Liu et al., 2018; Yin et al., 2008).

More recently, Liu et al. (2018) found that the antecedent precipitation amount (i.e., precipitation that contributed to soil moisture before plant growth began) strongly influenced vegetation productivity in arid and semi-arid regions at a global scale (the "water memory effect"). Dendroclimatic studies have indicated that tree-ring width were mainly influenced by antecedent precipitation and soil moisture for almost all main tree species (Cai and Liu, 2013; Cai et al., 2014, 2015; Gou et al. 2015; Fang et al., 2012; Liang et al., 2006; H. Liu et al., 2013; Y. Liu et al., 2017; Yin et al., 2008) and along elevations (Gou et al., 2005; Yang et al., 2013; Zhang et al., 2016) in the semi-arid region of China. In contrast, a warming climate can improve tree growth, since warming in the early or late growing season lengthens the growing season, and can also accelerate tree growth and increase forest biomass at some sites (Chen et al., 2019; Gao et al., 2018; McMahon et al., 2010; Salzer et al., 2009; Yang et al., 2017).

Based on this previous research, it appears that climate warming can affect stem radial growth differently in different areas due to both the direct effects of warming

and its interaction with moisture availability. However, detailed and locally specific conclusions and hypothetical mechanisms derived from *in situ* experiments or event-based observations are difficult to extrapolate to regional scales. As a result, regional studies tend to simplify or abstract the processes that control the interplay between climate and growth, creating uncertainty in the description or even paradoxes (Gao et al., 2018). These problems have delayed the development of process-based models and left the dynamic patterns of forest responses to drought and their underlying mechanisms unclear. Thus, there are research gaps on how climate change will affect future stem radial growth.

The development of simplified but process-based forward models of tree-ring formation could offer a valuable tool for understanding the non-linear mechanisms of stem radial growth and their responses to climate variables. Accounting for such processes would help us develop better predictions of future tree growth (Anchukaitis et al., 2006; Evans et al., 2006; Fritts, 2001; Li et al., 2014; Gonzalez-Benecke et al., 2017; Misson et al., 2004; Shishov et al., 2016; Tolwinski-Ward et al., 2011, 2013; Vaganov et al., 2006, 2011). The Vaganov–Shashkin-Lite model (hereafter, VS-Lite; Tolwinski-Ward et al., 2011, 2013) is one of the simplest available nonlinear and realistically multivariate models of the response of stem radial growth to climate at a regional scale. It permits comparison to a widely observed measurement for hindcasting/validation exercises using data from the 20th century (Breitenmoser et al., 2014). It only requires the following as input variables: site latitude, monthly mean

111 temperature, and monthly total precipitation (Tolwinski-Ward et al., 2011). The
112 VS-Lite model has successfully simulated regional patterns of climate limitation of
113 stem radial growth in a range of environments from semi-arid to temperate and boreal
114 regions (Breitenmoser et al., 2014; Chen et al., 2017; Lavergne et al., 2015; Mina et
115 al., 2016; Sanchez-Salguero et al., 2017a, 2017b; Tumajer et al., 2017). However,
116 because tree responses to climate are nonlinear and not fully understood, the model's
117 applicability to certain climate zones is unclear.

118 In the present study, we sought to clarify how tree stem radial growth responds to
119 different climate patterns based on 33 tree-ring chronologies from China's semi-arid
120 region. Our goal was to forecast radial growth under various climate scenarios using
121 the VS-Lite model. Specifically, we considered the IPCC "representative
122 concentration pathways" (RCPs), which are climate projections that cover a wide
123 range of possible changes in future anthropogenic greenhouse gas emissions (Collins
124 et al., 2014). Since about 1960, China's semi-arid region has been subject to different
125 precipitation patterns, with an overall wetting trend in the west and overall drying
126 trend in the east, due to fluctuation of the Asian Summer Monsoon (Yang et al., 2014).
127 Thus, it represents an ideal region for assessing the spatial heterogeneity of climate
128 responses. Our specific objectives were to (1) investigate relationships between stem
129 radial growth and climate change in the semi-arid region of China; (2) explore the
130 stem radial growth response to extreme drought events and quantify the relative
131 contributions of growing season soil moisture and temperature to stem radial growth

responses in the two sub-regions; and (3) forecast stem radial growth trends in the sub-regions under different climatic forcing scenarios projected for the remainder of the 21st century. We hypothesized that (1) stem radial growth would be mainly influenced by precipitation-induced changes in moisture availability in semi-arid China; (2) stem radial growth in the drying eastern sub-region would be more vulnerable to drought than in the increasingly humid western sub-region; and (3) rising temperatures will enhance growth by prolonging the growing season in both sub-regions under the projected climate scenarios.

2. Materials and methods

2.1 Study region

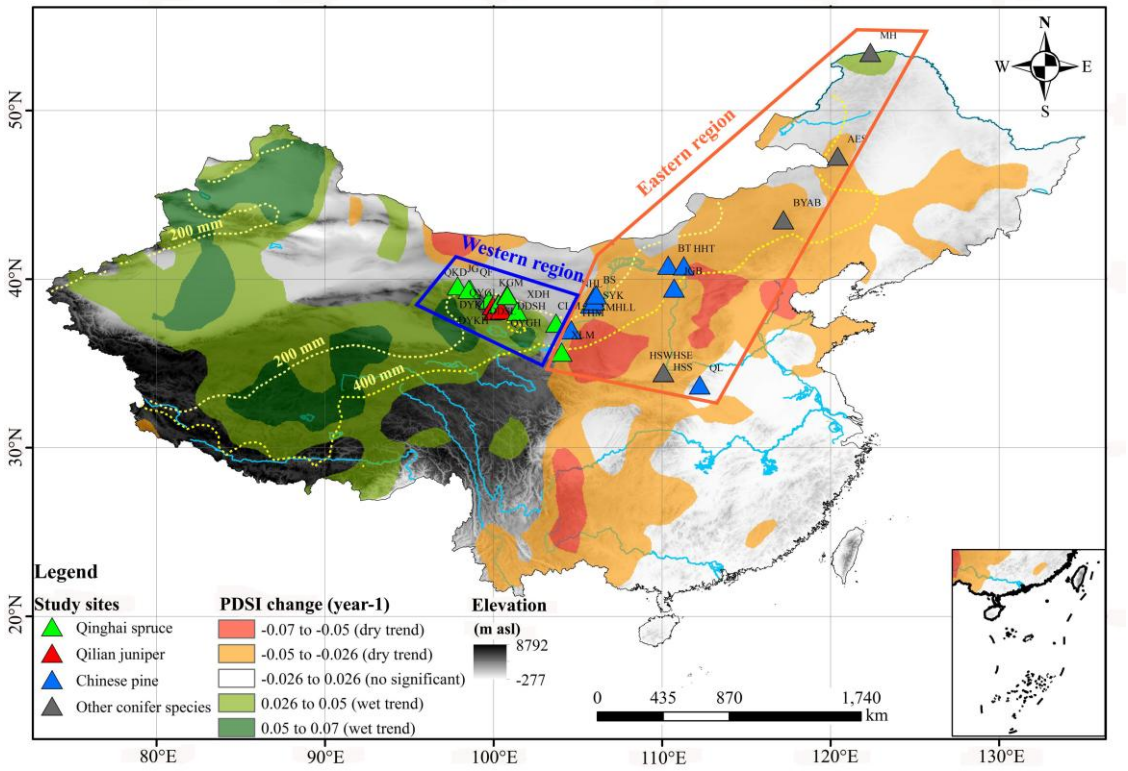

Figure 1 Map showing the locations of the study sites and moisture trends. Colors show the linear rate of change of the annual mean CRU self-calibrated Palmer

Drought Severity Index (scPDSI) from 1960 to 2013 throughout the study region (based on data downloaded from https://climexp.knmi.nl/). The red and green colors indicate significant negative (drier) and positive (wetter) trends, respectively, based on the 95% confidence interval. The dotted yellow lines indicate mean annul total precipitation isoline which based on gridded precipitation dataset of Global Precipitation Climatology Centre from 1960 to 2013 (data downloaded from https://www.esrl.noaa.gov/psd/data/gridded/data.gpcc.html).

The study region covers the central and eastern parts of China's semi-arid region and the surrounding regions (Figure 1). The topography is dominated by the Greater Hinggan Mountains, Qinling Mountains, Huashan Mountains, Yinshan Mountains, Erdos Plateau, Helan Mountains, and Qilian Mountains. The region's climate depends strongly on elevation and latitude; because the elevation ranges from below sea level to nearly 8800 m asl and the latitude covers a range of roughly 20°, there are large spatial gradients in both temperature and precipitation. According to statistical data obtained from local meteorological stations from 1960 to 2013, the mean growing season temperatures (April to October) range from -8.1 to 21.7°C, and the total growing season precipitation ranges from 76 to 698 mm (Table S1). To test Yang et al.'s (2014) assertion about the regional climate trends, we calculated the trends from 1960 to 2013 for the annual mean Climatic Research Unit (CRU) self-calibrated Palmer Drought Severity Index (scPDSI) based on the CRU scPDSI data downloaded from https://climexp.knmi.nl/ using linear interpolation (Figure 1). Our results confirmed that the western and eastern parts of our study region show different trends, with most of the eastern sub-region becoming significantly drier, and most of the

168 western sub-region becoming significantly wetter. Accordingly, we divided the
169 semi-arid region into two parts at about 104°E (Figure 1).

170 **2.2 Tree-ring data**

171 We used a total of 33 tree-ring width chronologies for six major conifer species
172 (*Picea crassifolia*, *Juniperus (Sabina) przewalskii*, *Pinus tabulaeformis*, *Pinus*
173 *armandii*, *Picea mongolica,* and *Larix gmelinii*) in the present study (Table S1). For
174 sites BS, SYK, and BYAB, we obtained two increment cores per living tree from 24
175 trees per site in the western and eastern Helan Mountains and in the Baiyinaoba
176 National Forest Reserve in September 2013, respectively. For sites AES and MH, we
177 obtained two increment cores per living tree from 25 trees per site in the Aer
178 Mountains and the Greater Hinggan Mountains in September 2014. All other tree-ring
179 samples and tree-ring width chronologies were obtained from the literature (see Table
180 S1), either by personal communication with the authors or by downloading the data
181 from the International Tree-Ring Data Bank
182 (https://www.ncdc.noaa.gov/data-access/paleoclimatology-data/datasets/tree-ring).
183 For each sample site, we obtained climate data from the nearest meteorological station
184 (Table S2). Distance between sample sites and meteorological stations range from 2 to
185 98 km, and elevation differences range from 15 to 1539 m a.s.l.

186 The sampling sites were distributed at elevations ranging from 348 to 3550 m asl.
187 Tree-ring growth patterns were generally consistent across species and spatially
188 coherent (Figure S1; Liu et al., 2013). At each site in the present study, the sample

189 included at least 19 standing dominant or codominant trees. Radial growth was
190 measured in two to three radial cores per tree, which were extracted with an increment
191 borer at breast height (1.3 m) from the cross-slope sides of the stem whenever
192 possible (Fritts, 2001). Wood samples were sanded until the rings were visible and
193 then visually cross-dated. Once dated, the tree-ring widths were measured to the
194 nearest 0.01 mm using a binocular microscope and a LINTAB measuring device
195 (Rinntech, Heidelberg, Germany). The accuracy of the visual cross-dating and
196 measurements were checked using the COFECHA software (Holmes, 1983). We then
197 used negative exponential or linear regression models to detrend the age series for
198 each tree and finally averaged the detrended tree-ring series to produce a standard
199 tree-ring width chronology using the ARSTAN software (Cook, 1985). We selected
200 the chronologies after the year 1960 for further analyses, as this period corresponds to
201 the period of reliable climatic data for the study area.

202 **2.3 Climate data**

203 Monthly mean temperature and precipitation data were obtained from the China
204 National Meteorological Information Center (http://data.cma.cn/) for the
205 meteorological stations nearest to the sampling sites for the period from 1960 to 2013.
206 Correction for elevation differences requires knowledge of the site-specific
207 climatological lapse rate, which is difficult to achieve. For example, tests that
208 assumed a constant moist-adiabatic lapse rate on a site-by-site basis did not improve

209 the fits between tree-ring and model data, and as a result, this correction is no longer
210 generally performed (Breitenmoser et al., 2014).

211 Monthly-resolution predicted temperature and precipitation for the 21st century
212 were obtained from the downscaled dataset from the fifth phase of the Coupled Model
213 Intercomparison Project (CMIP5) with a 0.5°×0.5° spatial resolution
214 (http://gdo-dcp.ucllnl.org/downscaled_cmip_projections/). This dataset was processed
215 from raw data from 28 general circulation models (GCMs) using the bias-correction
216 spatial disaggregation method described in Brekke et al. (2013). Wang and Chen
217 (2014) found that the EC-EARTH model provided the best simulation of temperatures
218 and precipitation in China by comparing 35 climate models from CMIP5.
219 Consequently, we used the projected climate datasets from EC-EARTH as the input
220 data for our tree-ring model. We used data for the scenario (RCP 8.5) that most
221 closely tracked recent historical emissions (Lelieveld et al., 2016), as well as two
222 scenarios with lower emissions (RCP 2.6 and 4.5) in which the increase in annual
223 emissions is more gradual in the early 21st century and then slows after the mid-21st
224 century.

225 **2.4 Drought indices**

226 PDSI is one of most widely used drought indexes because of its strong
227 relationship with climate. The index is calculated by incorporating both monthly
228 precipitation and monthly air temperature into a soil water-balance model (Dai et al.,
229 2004; Palmer, 1965). We used the homogenized and quality-checked scPDSI datasets

(https://climexp.knmi.nl/) nearest to each sampling site for the period from 1960 to 2013 to provide a reliable data source across the whole study area. These datasets cover the global land surface (except for Antarctica) at a 0.5°×0.5° spatial resolution from January 1901 to December 2016.

Soil moisture can directly represent the balance between precipitation and evapotranspiration, surface runoff, and groundwater flow. In arid and semi-arid regions and also across most biomes (Klein et al. 2015), soil moisture is the factor that most directly controls tree growth (Yin et al., 2008). To calculate soil moisture in our study area, we used the monthly mean temperature and precipitation data as inputs for the National Oceanic and Atmospheric Administration's Climate Prediction Center (CPC) ''Leaky Bucket Model''. For details, see equations 1–3 in Huang et al. (1996). This scheme estimates evapotranspiration, surface runoff, and groundwater flow as empirical functions of the input data, and subtracts these losses from incoming precipitation plus the previous month's soil moisture to compute the present month's soil moisture (Tolwinski-Ward et al., 2011).

Much of the influence of temperature on the vulnerability of semi-arid forests to drought results from temperature's exponential influence on the atmospheric moisture demand (Liu et al., 2013), which is defined as the vapor-pressure deficit (VPD). VPD represents the saturation vapor pressure minus the actual vapor pressure. We estimated the monthly VPD values from 1960 to 2013 for each sampling site using the methods of Hogg (1997) and Hogg et al. (2013). The mean VPD can be estimated

from the saturation vapor pressure (kPa) at the monthly mean values of the daily maximum temperature ($e^*_{T\max}$), minimum temperature ($e^*_{T\min}$), and dewpoint temperature ($e^*_{T\mathrm{dew}}$):

$$VPD = 0.5\times(e^*_{T\max} + e^*_{T\min}) - e^*_{T\mathrm{dew}} \quad (1)$$

Where $e^*_{T\mathrm{dew}}$ represents the relationship between air temperature (T, °C) and saturated vapor pressure, $e^*_{T\mathrm{dew}} = e_0 \times 10^{(7.5T/[\mathrm{T}+237.3])}$, and the value of e_0 was 0.611 kPa, and T was the mean monthly maximum (max) or minimum (min) temperature. Mean monthly T_{dew} was estimated as the saturation vapor pressure at the monthly mean value of $T_{\min}$ minus 2.5°C (Hogg, 1997). Daily maximum and minimum temperatures were obtained from the meteorological stations nearest to the sampling sites for the period from 1960 to 2013 (http://data.cma.cn/).

2.5 VS-Lite model

We used the VS-Lite model and a Bayesian parameter estimation approach to simulate tree-ring width indices (TRWi) for each site (Tolwinski-Ward et al., 2013; http://www.ncdc.noaa.gov/paleo/softlib/softlib.html). The model uses the CPC "Leaky Bucket model" (Huang et al., 1996) to estimate monthly soil moisture from temperature and total precipitation data. For each year, the model simulates standardized tree-ring width anomalies from the minimum of the monthly growth responses to temperature (g_{T}) and moisture (g_{M}), modulated by insolation (g_{E}). Day length is determined from the site latitude and does not vary from year to year on a given date. g_{T} and g_{M} in VS-Lite involve only two parameters. The first parameter

272 represents the temperature (T_1) or soil moisture (M_1) threshold below which growth
273 will not occur, and the second is the optimal temperature (T_2) or soil moisture (M_2)
274 above which growth is not limited by climate. The CPC "Leaky Bucket model"
275 includes nine parameters, but Tolwinski-Ward et al. (2011) have argued that
276 simulations are not terribly sensitive to the values of these parameters. Consequently,
277 we estimated the values of only four parameters (T_1, T_2, M_1, and M_2) using a Bayesian
278 parameter estimation approach (Tolwinski-Ward et al., 2013). This scheme assumes
279 uniform priors for the growth-response parameters and independent, normally
280 distributed errors for the modeled TRWi values. We used the posterior median for
281 each parameter to obtain the "calibrated" growth response for a given site. Finally, we
282 ran the model over the entire period from 1960 to 2013 using the calibrated
283 parameters for each site to produce a simulated tree-ring chronology that represented
284 an estimate of the site-specific climate signal that controlled stem radial growth. A
285 more detailed description of the approach can be found in the study by
286 Tolwinski-Ward et al. (2013).

287 Temperature (T_1, T_2) and soil moisture (M_1, M_2) growth parameters were
288 sampled uniformly between the maximum and minimum values, and we used the
289 growth parameter set that produced the simulation that correlated most strongly with
290 the corresponding observed TRWi series for each site in the simulations. In addition,
291 we obtained the values of other parameters (e.g., soil moisture, runoff, and root depth)
292 from Tolwinski-Ward et al (2011, 2013). We evaluated the model 10 000 times for

each site using three parallel Markov-chain Monte Carlo chains with a uniform prior distribution for each parameter and a Gaussian white noise model error (Tolwinski-Ward et al., 2013). To compute annual TRWi values, we integrated the overall simulated growth rates (i.e., the point-wise minimum monthly g_T, g_M, and g_E) over the time window from September of the year before tree-ring formation to October of the year of tree-ring formation. This choice results in comparable levels of autocorrelation in the observed and simulated site series (Sánchez-Salguero et al., 2017b; Tolwinski-Ward et al., 2011; Tumajer et al., 2017).

To test the temporal stability of the model results, we ran 100 calibration and validation tests for each sampling site, with each calibration interval chosen as a random half subset of the length of tree-ring chronology in each sampling site. We computed an index of stability (I_S) at each site in the network to compare the dependence of the models on the calibration-interval tuning. We defined this index as 1 minus the mean absolute change in the level of correlation significance p value of the simulation with observation from the calibration to validation interval across the 100 Monte Carlo tests (Tolwinski-Ward et al., 2011):

$$I_s(\text{site}_j) = 1 - \frac{1}{100}\sum_{i=1}^{100}\left|p_{\text{cal}}^{i,j} - p_{\text{val}}^{i,j}\right| \qquad (2)$$

where I_S (site$_j$) represents the index of stability for site j, "cal" represents the correlation significance between the calibrated values for sites i and j, and "val" represents the correlation significance between the validation values for sites i and j. I_S therefore ranges between 0 and 1, with values closer to 1 indicating greater model

stability outside of the calibration window. Note that this metric is defined in terms of changes in a measure of simulation quality from the calibration to the validation interval, but contains no information about the absolute simulation quality.

Finally, we ran VS-Lite models for each site using the calibrated parameters and projected monthly precipitation and mean temperature to obtain a simulated TRWi series for the period from 2014 to 2100 under the three RCP scenarios.

2.6 Statistical analysis

We assessed the relationships between the monthly climate data (mean temperatures and precipitation), drought indices (CRU scPDSI, soil moisture, VPD), and TRWi by calculating Pearson's correlation coefficient (r) for the relationships between pairs of variables for the common period from 1960 to 1987. The temporal window for the growth-climate comparisons extended from the previous May to the current October. We also examined composite periods within this range, such as from the previous August to the current July and from April to June of the current growing season. To determine the main climatic factors that limited tree growth, we also calculated the proportions of the long-term chronologies that were significantly correlated ($P < 0.05$) with the environmental variables for each month.

To assess the sensitivity of stem radial growth in the eastern and western sub-regions of our study area to extreme drought, we calculated "pointer" years for the two sub-regions that represented years with an abrupt change in climate. Pointer years are an accepted method of showing annual growth reactions that result from

abrupt changes in environmental conditions (Schweingruber et al., 1990), especially due to climatic variations (Neuwirth et al., 2007).Therefore, we transformed all TRWi values from the two sub-regions into an annual resolution high-frequency time series of pointer values using a two-step approach. First, we calculated the ratio of the TRWi for a given site to its 5-year moving average according to the method of Cropper (1979). These Cropper values were then normalized to have a mean of 0 and a standard deviation of 1 for the period from 1960 to 2013. We defined the thresholds for these Cropper values, which we used to identify extreme-climate event years, using the method of Neuwirth et al. (2007). That is, if C represents the normalized Cropper value, $|C| > 1$ represents a weak change, $|C| > 1.28$ represents a strong change, and $|C| > 1.645$ represents an extreme change. We defined a negative (positive) pointer year as a year when at least 50% of all TRWi values within a sub-region showed a negative or positive extreme event year. We then compared the mean g_T and g_M between negative pointer years and positive pointer years for the two sub-regions from January to December. We used independent-sample t-tests to identify significantly different means of g_T and g_M between negative pointer years and positive pointer years in the two sub-regions. Data were log-transformed (log [x+1]) when the distribution diverged from normality according to the Shapiro-Wilks test.

To quantify the contribution of soil moisture and temperature to the simulated TRWi, we divided each year into two parts: first, months when growth was controlled by soil moisture ($g_M < g_T$), and second, months when growth was controlled by

temperature ($g_M > g_T$), and then calculated the ratio of the integrated relative growth rate (G_r) controlled by soil moisture and temperature each year:

$$M_C = \frac{\sum gE(s_M)*gM(s_M)}{\sum_{s=1}^{12} gE(s)*\min\{gM(s)|gT(s)\}} \quad (3)$$

$$T_C = \frac{\sum gE(s_T)*gT(s_T)}{\sum_{s=1}^{12} gE(s)*\min\{gM(s)|gT(s)\}} \quad (4)$$

Where M_c and T_c represent the contributions of soil moisture and temperature, respectively, to simulated TRWi, and s, s_M, and s_T represent every month, a month controlled by soil moisture, and a month controlled by temperature, respectively. We then used independent-sample t-tests to identify significant mean differences of M_c and T_C between the two sub-regions during the study period from 1960 to 2013. Data were log-transformed (log [x+1]) when the distribution diverged from normality according to the Shapiro–Wilks test.

Unless otherwise noted, we used version R2012b of the MATLAB software (https://www.mathworks.com/) for all VS-Lite simulations and for statistical analyses of the data.

3. Results

3.1 Stem radial growth trends in the two sub-regions

The TRWi records were generally consistent within and between the western and eastern sub-regions from 1901 to 1960 (r = 0.57, n =59, P < 0.001; Figure S2). Both sub-regions recorded low TRWi from the late 1920s to the early 1930s (Figure S2).

However, their coherence decreased markedly from 1960 to 2013 (r = 0.30, n =53, P < 0.05; Figure S2). We observed a statistically significant trend of increasing growth in the western sub-region (*slope* = 0.005, R^2 =0.18, P < 0.01). In contrast, we detected a slightly decreasing but not statistically significant trend in the eastern sub-region (Figure S2).

3.2 Relationship between stem radial growth and climate

We detected high common site-to-site variation in the climate–growth relationships within each sub-region, especially for the western sub-region (Figure 2b, S3). We found no significant correlation between TRW_i and temperature in both sub-regions (Figure 2a). In contrast, we found a common significant positive influence of the antecedent precipitation conditions (from the previous August to the current July) on current TRW_i in both sub-regions. Furthermore, we also found strong correlations with precipitation in the early growing season (from the current April to June) in both sub-regions (Figure 2b). Similarly, we found a common significant positive influence of CRU scPDSI and soil moisture in both sub-regions (Figure 2c.d). TRW_i values were significantly positively correlated with the average CRU scPDSI and soil moisture from April to June of the current year and from the previous August to the current July. However, we also found significant positive correlations for scPDSI in May and June of the current year and for soil moisture in June of the current year. The correlations between TRW_i and VPD were not significant for most sites in both sub-regions in most months (Figure 2e). The most significant correlations

were found in the current June, with about 48% of the chronologies from the study region showing significant negative correlations with the June VPD ($P < 0.05$; Figure 2e). In addition, TRW_i at some sites (41% of the total) was significantly negatively correlated with VPD in September of in the previous year.

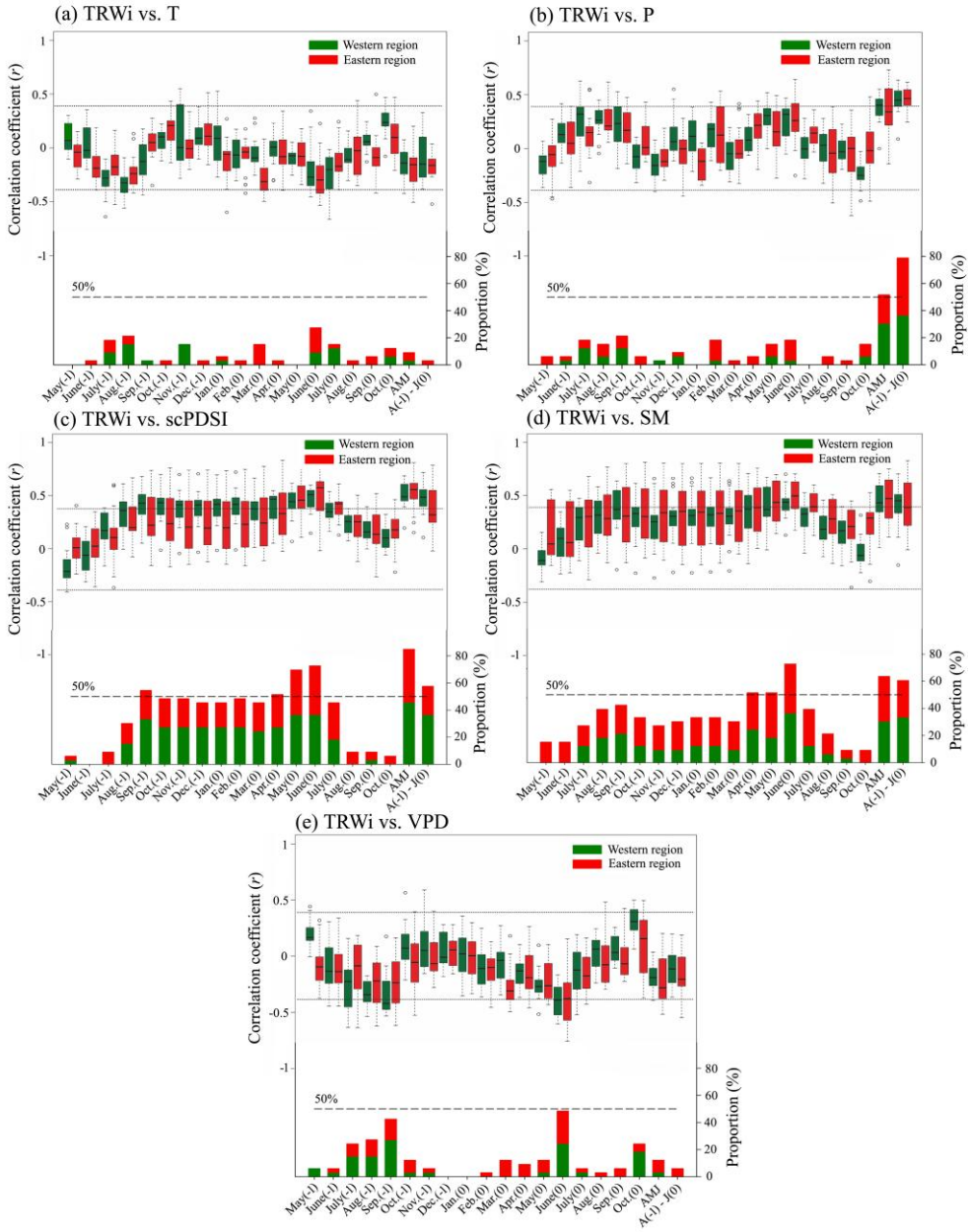

Figure 2 Box plots for Pearson's correlation coefficient (r) for the relationship between the tree-ring width indices (TRWi) in the western and eastern sub-regions and the climate variables (top panel) and the proportion of the sites in the time series

for which we detected a statistically significant ($P < 0.05$) correlation with the climate variables (bottom panel) from May of the previous year (denoted -1 for all months in the previous year) to October of the current year (denoted 0 for all months in the current year), as well as for the period from April to June (AMJ) in the current growing season and from the previous August to the current July (A(-1) – J(0)). (a) TRWi vs. temperature (T), (b) TRWi vs. precipitation (P), (c) TRWi vs. the self-calibrated Palmer drought severity index (scPDSI), (d) TRWi vs. soil moisture (SM), and (e) TRWi vs. the vapor-pressure deficit (VPD). The horizontal dotted lines in the upper panels indicate the 95% confidence interval. Box plots describe the spread of data: median value (bold black horizonal line), upper and lower quartiles (boxes), and the lower and upper extremes (whiskers), beyond which outliers are plotted as dots.

3.3 Model results: non-linear effects of climate factors on stem radial growth

The VS-Lite model simulated the year-to-year variability in TRW_i during the study period from 1960 to 2013 with reasonable accuracy (Table 1). The correlation coefficients between the observed and simulated TRW_i were significant ($P < 0.05$) for all sites, and ranged from 0.41 to 0.75 (Table 1). The Bayesian estimated growth response parameters (T_1, T_2, M_1, and M_2) were similar among all study sites (Table S3). Furthermore, we found high coherency between the mean observed and simulated TRW_i in both sub-regions; for all sites combined, the correlations were significant ($P < 0.001$) and high, with r values of 0.70 for the west and 0.77 for the east (Figure 3a, b). Calibration and validation tests further demonstrated the temporal stability of the model results. We found similar and significant mean correlation coefficients between the modeled and observed TRW_i for the calibration and

validation periods for most sites, with mean I_S values of 0.86 and 0.78 in the western and eastern sub-regions, respectively, which suggests that the model results are only weakly influenced by tuning of the calibration interval (Table S4).

Table 1 Values of Pearson's correlation coefficient (*r*) for the relationships between the observed standardized tree-ring width chronologies and the modeled tree-ring series based on the Bayesian parameter estimation method. Significance: $^{n.s.}$ not significant, ** $P < 0.01$, ***$P < 0.001$.

Western region			Eastern region		
Chronology	**Correlation coefficient (*r*)**	**Degrees of freedom (*df*)**	**Chronology**	**Correlation coefficient (*r*)**	**Degrees of freedom (*df*)**
QF	0.52***	42	XLM	0.58***	48
JG	0.53***	44	THM	0.49***	51
QKD	0.54***	44	MHLH	0.56***	36
KGM	0.52***	44	SYK	0.61***	52
SDLL	0.68***	51	BS	0.62***	52
SDLH	0.65***	51	NHL	0.59***	38
ZMSH	0.70***	51	MHLL	0.62***	36
ZMSL	0.71***	51	HSS	0.75***	44
DYKL	0.54***	51	HSW	0.71***	44
DYKH	0.56***	51	HSE	0.45**	44
QYGH	0.51***	51	BT	0.70***	26
QYGL	0.51***	51	JGB	0.63***	38
DDSL	0.53***	42	HHT	0.61***	32
DDSH	0.61***	51	QL	0.43***	46
XDH	0.43***	44	BYAB	0.67***	52
CLM	0.49***	42	AES	0.48***	52
			MH	0.41**	52

The modeled g_T and g_M differed among the sub-regions (Figure 3a, b; Figure S4). However, the mean g_T, g_M, and G_r showed similar intra-annual patterns, although the absolute values of g_T, g_M, and G_r were higher in the eastern sub-region (Figure 3a,b). g_T peaked from June to August, whereas g_M increased during the summer, as expected,

in response to high precipitation brought by the Asian summer monsoon in both sub-regions. Tree growth was limited by low temperatures ($g_T < g_M$) at the beginning and end of the growing season, but by soil moisture availability ($g_M < g_T$) during summer and autumn (from May to September in the western sub-region; from May to August in the eastern sub-region; Figure 3a, b).

To further investigate how tree growth responds to moisture availability on a seasonal time scale, we examined the differences in mean g_T and g_M between negative and positive pointer years in the two sub-regions (Figure 3c, d). For the western sub-region, the negative pointer years were 1971, 1974, 1978, 1981, 1986, 1995, and 2001, whereas the positive pointer years were 1972, 1975, 1980, 1996, and 2002. For the eastern sub-region, the negative pointer years were 1966, 1987, and 2000, whereas the positive pointer years were 1970, 2002, and 2009. With regard to the mean g_T profile, there was no significant difference between negative and positive pointer years in both sub-regions (top panels of Figure 3c, d). With regard to the mean g_M profile, there was a significant difference between negative and positive pointer years in the eastern sub-region in the early growing season (April to June, $P < 0.01$), versus no significant difference in the western sub-region (bottom panel of Figure 3c, d).

Finally, we compared the contribution of soil moisture to the simulated stem radial growth in the two sub-regions (Figure 3e). We found that the mean contribution of soil moisture in the eastern sub-region was significantly higher than that in the western sub-region (77% vs 69%, respectively), whereas the mean contribution of soil

461 temperature in the eastern sub-region was significantly higher than that in the western
462 sub-region (23% vs 31%, respectively; data not shown). For the inter-annual variation
463 of the mean contribution of soil moisture, we found a slight but significant increasing
464 trend for the contribution of soil moisture from 1960 to 2013 in the eastern sub-region
465 (slope = 0.077, $P = 0.01$), but no significant trend in the western sub-region.

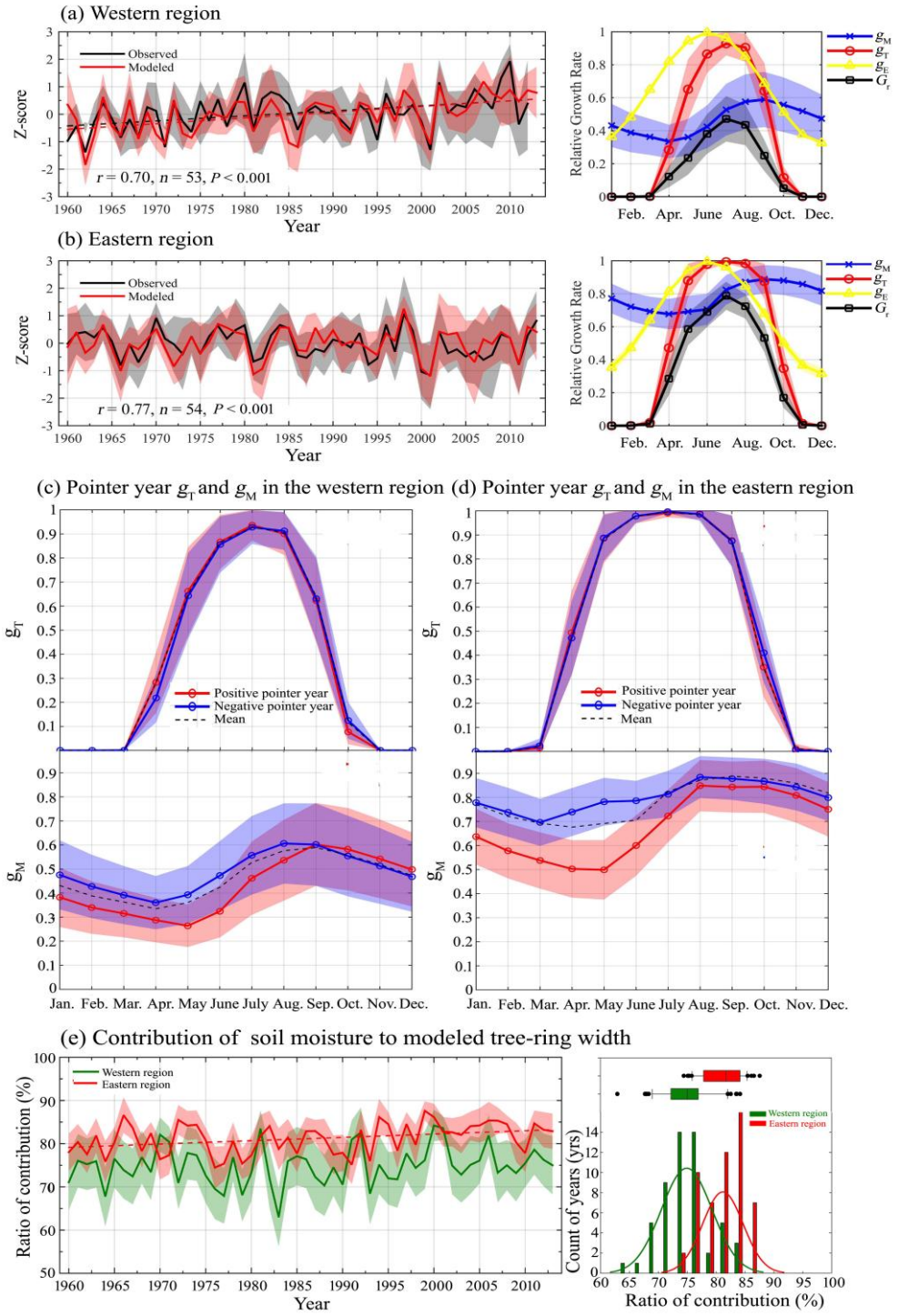

Figure 3 Comparisons between modeled and actual values of the tree-ring width index (normalized *z* values) for the (a) western and (b) eastern sub-regions of semi-arid China and (right panels in both figures) the corresponding mean pattern produced by the VS-Lite model for the simulated mean temperature (g_T), soil moisture

(g_M), and solar irradiation (g_E) response functions and integrated relative growth rates (G_r) from January to December (right panel). Comparisons of positive and negative pointer years for the modeled mean g_T (top panel) and g_M (bottom panel) in the (c) western and (d) eastern sub-regions. (e) Inter-annual variation of the calculated mean contributions of soil moisture to the modeled tree-ring width indices, and (right panel) the box plots and distribution of the contribution values in the western and eastern sub-regions from 1960 to 2013. Shaded areas represent the mean ± 2SE. In (a), dashed lines represent significant positive trends over time for the observed and modeled TRWi values for the western sub-region ($y = 0.018x - 26.23$, $P < 0.01$ for mean observed TRWi; $y = 0.021x - 41.39$, $P < 0.001$ for mean modeled TRWi) determined by piecewise linear regression. In (e), we also detected a significant positive trend for the inter-annual variation of the contribution of soil moisture to the modeled TRWi in the eastern sub-region ($y = 0.077x - 71.45$, $P = 0.01$), which was determined by piecewise linear regression. The black dotted lines in (c) and (d) represent the average g_T and g_M over the full period (1960 to 2013). Box plots in (e) describe the spread of data: median value (bold black horizonal line), upper and lower quartiles (boxes), and the lower and upper extremes (whiskers), beyond which outliers are plotted as dots.

3.4 Projected growth responses to climate warming

The warmer conditions projected by the three climate scenarios (RCP 2.6, 4.5, and 8.5) predict a slight but significant increasing mean TRWi in the two higher emission scenarios (RCP 4.5 and 8.5) in both sub-regions (all $P < 0.05$; Figure 4).

The projected growth responses to temperature (g_T) and soil moisture (g_M) were similar for the three emission scenarios. Similar to the recent situation (1960 to 2013), the projected g_T peaked from June to August, whereas g_M increased during the summer, as expected, in response to the high precipitation during this season. Tree growth was limited by low temperatures ($g_T < g_M$) at the beginning and end of the growing season and by soil moisture availability ($g_M < g_T$) during the summer and autumn (from May to September in the western sub-region; from May to August in the eastern sub-region; see Figure 4).

The projected growth in both sub-regions was still mainly controlled by soil moisture under all climate scenarios (ratio of contribution > 80%; Figure S5). Furthermore, we found significant increasing trend of mean contribution of soil moisture for all climate scenarios from 2014 to 2100 in both sub-regions, except for the western sub-region under RCP 2.6 (Figure S5).

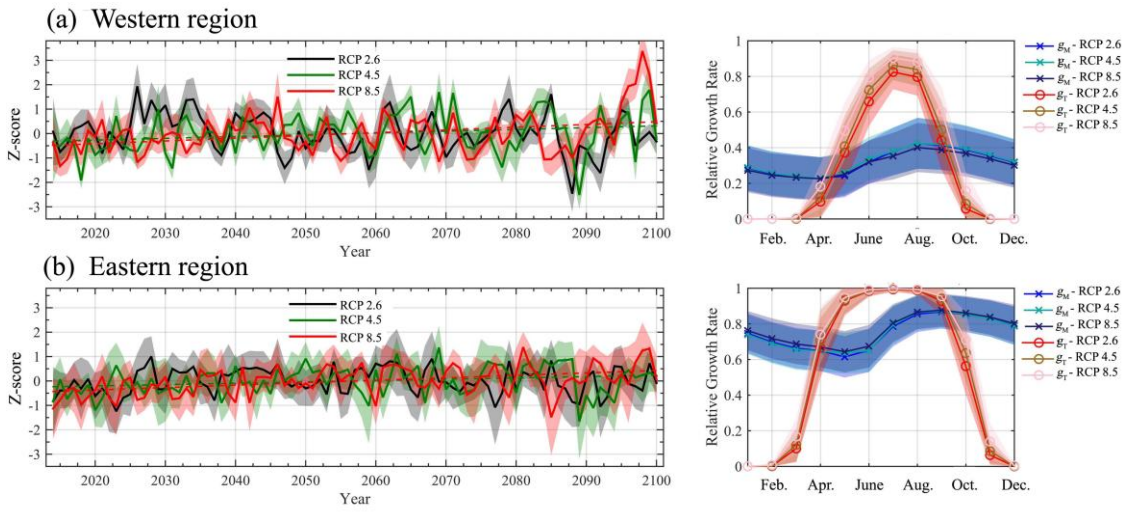

Figure 4 Comparison of the responses of the mean modeled tree-ring width indices (TRW_i) under different IPCC emission scenarios (RCP 2.6, 4.5, and 8.5) for the projected period from 2014 to 2100 in the (a) western and (b) eastern sub-regions of

semi-arid of China, and (right panels) the corresponding mean pattern of the VS-Lite simulated mean temperature (g_T), soil moisture (g_M), and solar irradiation (g_E) response functions and partial growth rates (G_r) from January to December. The shaded areas represent the mean ± 2SE. We detected a significant positive trend in the mean projected TRWi based on the VS-Lite model in the western region in two scenarios ($y = 0.007x - 15$, $P < 0.05$ for RCP 4.5; $y = 0.011x - 23.14$, $P < 0.01$ for RCP 8.5), determined by piecewise linear regression (dotted green and red lines, respectively). We also detected a significant positive trend in the mean projected TRWi based on the VS-lite model in the eastern region in the same scenarios ($y = 0.005x - 11.18$, $P < 0.05$ for RCP 4.5; $y = 0.01x - 20.54$, $P < 0.001$ for RCP 8.5), determined by piecewise linear regression (dotted green and red lines, respectively).

4. Discussion

In this study, the tree-ring data demonstrated that tree growth in the semi-arid region of China is mainly affected by precipitation, and showed a significant "water memory effect". Tree growth rates in the western and eastern sub-regions showed divergent trends, possibly caused by different precipitation patterns since 1960. Tree growth in the eastern sub-region is more vulnerable to extreme drought events than in the western sub-region. Our forecasting results showed a slight but significant trend of increasing tree growth under the two higher emission scenarios (RCP 4.5 and 8.5) in both sub-regions, which might be related to the prolongation of the growing season caused by climate warming.

Our first hypothesis was confirmed by the results, which revealed that stem radial growth was mostly influenced by precipitation. Drought can limit tree growth in two ways: (1) increased evaporative demand caused by climate warming, known as

533 “global-change-type” drought (Breshears et al., 2005), and (2) a lack of precipitation,
534 known as “precipitation-induced” drought. Our correlation analysis indicated that
535 tree-ring width increased with increasing precipitation, PDSI, and soil moisture from
536 the previous August to the current July, but was only weakly correlated with
537 temperature and VPD (Figure 2). The stronger influence of precipitation and weaker
538 influence of VPD suggest that tree growth in the study region is mainly controlled by
539 the second aspect of drought (i.e., a precipitation shortage). Under conditions of low
540 precipitation or limited soil moisture, trees respond with reduced cell growth rates
541 (Chaves et al., 2002; Popkova et al., 2018), smaller cell lumen areas (Belien et al.,
542 2012), or reduced wood growth rates (Arend and Fromm, 2007).

543 The tree-ring width chronologies also showed significant correlations with
544 precipitation or soil moisture records in previous studies of China’s arid and semi-arid
545 regions (Cai et al., 2015; Liu et al., 2017; Yang et al., 2014; Yin et al., 2008). In
546 contrast, most previous studies conducted in other drought-prone regions indicated
547 that tree-ring growth was mainly influenced by heat-induced drought (Gao et al., 2018;
548 Liu et al., 2013; Peng et al., 2011; Williams et al., 2010, 2013; Wu et al., 2013, 2018).
549 Williams et al. (2013) found that tree-ring width in the southwestern United States
550 was mainly influenced by the warm-season VPD (which is largely controlled by
551 temperature). Sánchez-Salguero et al. (2017b) found that rising temperatures could
552 amplify drought stress and thus constrain the radial growth of circum-Mediterranean
553 fir forests. Liu et al. (2013) suggested that tree growth was significantly affected by

554 warming-induced increases in atmospheric moisture demand in the semi-arid regions
555 of Inner Asia. The difference between these studies and our results might have been
556 caused by several factors.

557 First, differences in climatic conditions would affect the results. The research by
558 Williams et al. (2013) and Sánchez-Salguero et al. (2017a, 2017b) was conducted in
559 regions with a Mediterranean climate and a continental influence, characterized by
560 warm and dry summers and cool and wet winters. Liu et al. (2013)'s study sites were
561 mainly distributed in northern Mongolia, which is subjected to a temperate continental
562 climate characterized by warm and dry summers and cold winters. In contrast, our
563 sampling sites are mainly influenced by the Asian summer monsoon, which is
564 characterized by warm and wet summers and cold and dry winters. Warm and dry
565 summers could increase atmospheric water demand but decrease soil water
566 availability (i.e., supply < demand), thereby exacerbating the effects of water stress
567 upon tree growth. In contrast, the warm and wet summer climate could both increase
568 atmospheric demand and increase or leave unchanged soil water availability (i.e.,
569 supply > demand), thereby causing tree growth to be affected more strongly by the
570 water supply.

571 Secondly, many studies may have underestimated the real sensitivity of
572 vegetation to precipitation variability by considering only the effects of short-term
573 precipitation on vegetation growth during the same season (Huete, 2016; Ji and Peters,
574 2003). In contrast, our results demonstrated the importance of precipitation in the year

575 before ring growth. That is, we found that current vegetation productivity was more
576 strongly affected by antecedent precipitation ("water memory effects") than by
577 contemporary precipitation in China's semi-arid region. This agrees with previous
578 research (Liu et al., 2018).

579 Recent studies have indicated that "water memory effects" play a more
580 significant role than was previously believed in influencing the vegetation
581 productivity of arid and semi-arid regions (Liu et al., 2018; Peltier et al., 2018; Shen
582 et al., 2016; Wu et al., 2015). For example, Liu et al. (2018) found that vegetation
583 productivity depended greatly on antecedent precipitation in arid and semi-arid
584 regions, and the average length of water memory was approximately 5.6 months. This
585 was comparable to a previous study in which vegetation in arid and semi-arid regions
586 was most sensitive to water anomalies for about 4 to 6 months (Lotsch et al., 2003). A
587 longer (12-month) response to antecedent precipitation was also identified in arid
588 regions such as the central-western United States and central Asia (Liu et al., 2018).
589 Consistent with these results, our study indicated that stem radial growth was
590 significantly positively correlated with precipitation from the previous August to the
591 current July (i.e., 11 months), but was not strongly or significantly correlated with
592 precipitation in any single month, which suggests the influence of a "water memory
593 effect". Liu et al. (2018) suggested that the "water memory effect" can be explained
594 by three factors: (1) the adaptation of vegetation to frequent water shortages by means
595 of relevant physiological mechanisms (Chaves et al., 2003; Vicente-Serrano et al.,

2013); (2) a lagged vegetation response to soil moisture anomalies in arid or semi-arid regions (Chen et al., 2014; Richard et al., 2008); and (3) hierarchical responses of vegetation to resource availability (i.e., different response strengths for different strengths of resource availability) (Schwinning and Sala, 2004). In addition, antecedent precipitation could influence the activity of stored nonstructural carbohydrates (Gao et al., 2018), and the role of stored nonstructural carbohydrates in drought resistance has been studied in a semi-arid pine forest (Klein et al. 2014). If there is enough water accumulation before the growing season, a tree can effectively turn these carbohydrates into new tissue when the temperature is suitable for growth to begin, leading to wider earlywood; if not, the carbohydrates would be consumed by metabolism. Most of sampling sites in our study (especially in the western sub-region) are located in areas over 2000 m a.s.l and are covered with snow-pack in winter. Higher winter precipitation (mostly in the form of snow) in the sampling site can increase the soil moisture content, compensating for water loss caused by drier spring conditions before summer rains begin (D'Arrigo and Jacoby, 1991; Li et al., 2016).

We found that TRWi values in the two sub-regions were slightly but significantly negatively correlated with VPD in the current June (Figure 2). This is consistent with previous studies in arid or semi-arid ecosystems (Liu et al., 2013; Williams et al., 2013). Warming early in the growing season could cause VPD to increase exponentially and soil moisture to decrease through evapotranspiration when moisture from the Asian summer monsoon has not yet reached the study region.

617 Increased VPD coupled with limited soil moisture increases the potential for strong
618 water stress, possibly including hydraulic failure (collapse of water columns within
619 xylem cells), and can force prolonged stomatal closure, thereby decreasing
620 photosynthesis, the plant's growth rate, and carbohydrate reserves (Adams et al., 2009;
621 McDowell et al., 2008; Williams et al., 2013). In addition, TRWi was slightly but
622 significantly negatively correlated with VPD in September of the previous year.
623 Although September is not entirely within the growing season, the mechanisms by
624 which the previous year's VPD limits tree growth are similar to those in the current
625 year. When conditions allow, photosynthesis continues during September after
626 cambial shutdown, allowing allocation of carbohydrates to reserves that influence
627 radial growth during the following growing season (Williams et al., 2013).

628 Our second hypothesis, in which stem radial growth in the drier eastern
629 sub-region is expected to be more vulnerable to drought than growth in the wetter
630 western sub-region, was also confirmed. In response to opposing moisture trends
631 since 1960, radial growth in the western and eastern sub-regions showed divergent
632 trends, with a significant increasing trend in the western sub-region, and a slight and
633 non-significant decreasing trend in the eastern sub-region (Figure S2). In addition, our
634 modeling results indicated that radial growth in both sub-regions was mainly
635 controlled by soil moisture, but the mean contributions of soil moisture to growth in
636 the eastern sub-region was significantly higher than in the western sub-region ($P <$
637 0.001). This might indicate that radial growth in the eastern sub-region is more

638 vulnerable to drought. Furthermore, the contributions of soil moisture in the eastern
639 sub-region show a significant increasing trend from 1960 to 2013 (Figure 3), which
640 indicate that radial growth in the eastern sub-region has become increasingly sensitive
641 to drought in the past half century. This hypothesis is supported by our pointer-year
642 analysis, which showed that g_M differed significantly between negative and positive
643 pointer years in the eastern sub-region during the early growing season (April to June,
644 $P < 0.01$), but not in the western sub-region (bottom panels of Figure 3c, d). In
645 addition, tree species and altitude might also influence the response tree-ring growth
646 to drought (Lévesque et al., 2014; McDowell et al., 2008; Sidor et al., 2015; Wang et
647 al. 2017). For this concern, we selected three main trees species used in the study
648 (*Picea crassifolia*, *Juniperus (Sabina) przewalskii,* and *Pinus tabulaeformis*) to test
649 the effect of species and altitude on tree-ring growth and it's climate responses
650 (Figure S6). Results indicated that no significant difference of tree growth and it's
651 climate responses between different elevations and species in the adjacent sampling
652 sites. In addition, we conduct linear mixed-effects analyses to detect if species and
653 elevation influenced tree-ring width significantly. We selected two most significant
654 climate variables (previous August to current July precipitation and April to June
655 PDSI) as fixed effects, and set species, elevation and site as random effects. Results
656 show that species and elevation are not critical for tree-ring growth ($P > 0.5$ for
657 Likelihood Ratio Test; Pinheiro and Bates, 2000).

Our sample species are dominated by *P. crassifolia* and *J. przewalskii* in the western region, whereas these species are rare in the east and are replaced by four additional species. However, a case study indicate tree-ring growth of *P. crassifolia* and *P. tabulaeformis* show similar response to soil water availability in the Helan Mountains, Northern Central China (data not published). Further studies to study the species-specific response to drought in this region may be beneficial in this context.

The significant increasing trend of radial growth since 1960 in the western sub-region has at least two potential causes. First, the trend of significantly wetter conditions could compensate for the increased evaporative demand caused by increasing temperatures, thereby alleviating drought stress and promoting tree growth (Gao et al., 2018). Second, the extended growing season could also increase radial growth of evergreen conifers (Gao et al., 2018; Körner and Basler, 2010; Pretzsch et al., 2014). Warmer climate could induce earlier initiation or later termination of radial growth (Gao et al., 2018; Yang et al., 2017). Previous studies indicated that lengthening of the growing season will increase tree growth (Chmielewski and Rötzer, 2001; Gao et al., 2018; Pretzsch et al., 2014). For example, Waring and Gao (2016) simulated the tree growth of Qinghai spruce using the process-based 3-PG forest model, and found that a recent reduction in the frequency of frost days during the growing season as a result of warming temperatures can explain the increased tree growth. Furthermore, this effect could be amplified by the higher contribution of temperature to radial growth (31%) in the western sub-region. In contrast, the slightly

679 declining radial growth in the past half century in the eastern sub-region might have
680 been caused by a combination of decreasing precipitation and increased evaporative
681 demand caused by increasing temperatures. Together, these processes could induce
682 drought stress that would decrease radial growth. In addition, the significant
683 difference of g_M between negative and positive pointer years in the eastern sub-region
684 during the early growing season might result from the combined effect of high
685 evaporative demand and low precipitation, which could together profoundly change
686 the soil water resources available for tree growth.

687 Our third hypothesis, that rising temperatures could enhance growth and prolong
688 the growing season in both sub-regions under the projected climate scenarios, was
689 also confirmed. We found that the warmer conditions projected by the scenarios
690 would lead to slightly but significantly increasing mean TRWi in the two scenarios
691 with higher emissions (RCP 4.5 and RCP 8.5) in both sub-regions (Figure 4, S5). We
692 hypothesize that the increasing trend might be mainly caused by increasing
693 temperatures at the beginning and end of the growing season, which would promote
694 tree growth by extending the growing season (Gao et al., 2018). This hypothesis is
695 supported by two factors: First, temperatures at the beginning (April) and end
696 (October) of the growing season showed significant increasing trends from 2014 to
697 2100 in the two higher emission scenarios (RCP 4.5 and RCP 8.5; Figure S7a-d).
698 Second, precipitation and soil moisture didn't show any significant increasing or
699 decreasing trends during the main growing season (May to September) from 2014 to

700 2100 in any emission scenario in both sub-regions (Figure S7e-h). However, we note
701 that temperature can only influence the long-term stem radial growth trend, and the
702 main factor is still soil moisture in both regions for the projected period from 2014 to
703 2100 (Figure 4).

704 Every modeling approach has limitations, assumptions, and drawbacks. We chose
705 the present methodological framework because it is relatively robust and provides
706 results that account for the non-linear mechanisms that underlie how tree growth
707 responds to climate change. Nevertheless, the VS-lite model has limitations (Lavergne
708 et al., 2015; Sanchez-Salguero et al., 2017b; Tolwinski-Ward et al., 2011, 2013). First,
709 the model fails to account for carry-over effects such as the water memory effect.
710 However, we found that precipitation conditions in the previous year strongly affect
711 current-year growth (Figure 2b). Ongoing monitoring of tree physiology,
712 environmental conditions, and wood cell formation to account for such memory
713 effects will provide a more detailed representation of the complex biological and
714 ecological processes that control tree growth in our study region. Second, our model
715 did not consider the influence of CO_2 on tree growth (the "CO_2 fertilization" effect).
716 Previous studies indicated that the growth responses to climate could be modulated by
717 species-specific reactions to rising atmospheric CO_2 concentrations, and this would
718 directly affect photosynthesis and improve water-use efficiency and thus growth
719 (Ainsworth and Long, 2005; Karnosky et al., 2003; Keenan et al., 2011; Liu et al.,
720 2007). Furthermore, CO_2 fertilization effects might compensate for the negative

721 effects of water stress at a short timescale, which also implies a non-linear response of
722 forest productivity to drought stress for semi-arid ecosystems such as those in our
723 study area (Poulter et al., 2014). In our study, we found a significantly increasing
724 trend for tree growth in the western sub-region, which might be further affected by
725 "CO_2 fertilization" (Wang et al., 2012, 2015). Third, the VS-Lite model inherits its
726 efficiency and robustness with respect to parameter choices from the rudimentary
727 CPC leaky-bucket model, but fails to account for winter precipitation stored in the
728 snow-pack (Tolwinski-Ward et al., 2011). Winter precipitation contributes to modeled
729 growth to some degree, especially for boreal and high-altitude mountain forests (Li et
730 al., 2016; Vaganov et al., 1999), as the soil moisture model contains significant
731 memory from month-to-month, but ring width variability at sites where winter
732 precipitation is the dominant control on growth are less likely to be realistically
733 represented by VS-Lite. Finally, extreme climatic events and biotic disturbances (e.g.,
734 cold or heat spells and insect or disease outbreaks caused by warming temperatures)
735 could also play important roles in driving forest vulnerability to climate change (Liu
736 et al., 2013). Several studies have highlighted that the susceptibility of trees to
737 extreme climatic events such as droughts is generally expressed by low growth rates
738 that do not surpass a critical threshold for net growth (Camarero et al., 2015a, 2015b).
739 Finally, we note that the results for tree growth projections are sensitive to
740 representative concentration pathway (RCP), and are only as predictive as these

741 scenarios realistically span the actual evolution of radiative forcing that occurs in the
742 future (Collins et al 2014).

743 **5. Conclusions**

744 We found that stem radial growth in our study region was mainly affected by soil
745 moisture availability. The divergent radial growth trends in the two sub-regions were
746 mainly influenced by different precipitation trends since 1960. In addition, increasing
747 temperature could also contribute to the increasing radial growth in the western
748 sub-region, where improving moisture conditions could compensate to some extent
749 for increased evapotranspiration under these conditions. Our use of a process-based
750 growth model let us define the vulnerability of stem radial growth to drought by
751 quantifying the relative contributions of soil moisture and temperature in the two
752 sub-regions. Tree-ring growth in the eastern sub-region appears to be more vulnerable
753 to drought than in the western sub-region. The two higher emission scenarios (RCP
754 4.5 and 8.5), which correspond to the most pronounced warming, show a predicted
755 slight growth increase in both sub-regions in the 21st century due to rising
756 temperatures at the beginning and end of the growing season.

757 In future research, it will be necessary to broaden the study area in the western
758 sub-region and select more sampling sites, especially in the eastern sub-region, to
759 validate the modeling results. In addition, since about half of the tree-ring
760 chronologies in our study end on or before 2005 which might exclude some of the
761 most important years of climate variability. In future, more tree-ring chronologies

762 which cover most recent years should be collected to validate our results. Finally,
763 studies based on more complicated tree ecophysiological models will be needed to
764 obtain a more realistic picture of forest responses to climate change in the study
765 region, and updated as the actual radiative forcing of climate proceeds.
766
767 **Acknowledgments**
768 This research was supported by the National Natural Science Foundation of China
769 (41571196, 41421061 & 41807431), by National Science Foundation of Shaanxi
770 Province (2019JQ-325), by the Fundamental Research Funds for the Central
771 Universities (GK201801007 and GK201903068), and by the Self-determination
772 Project of the State Key Laboratory of Cryospheric Sciences (grant SKLCS-ZZ-2019).
773 Dr. Xiaomin Zeng is grateful for the support from the China Scholarship Council and
774 the Department of Geology at the University of Maryland. We thank Dr. Mathias
775 Trachsel (University of Bern) for his assistance in the model calibration and
776 validation tests. We thank Prof. Jianguo Huang for his comments on the manuscript.
777 We thank Geoff Hart for providing language help. We gratefully acknowledge the
778 journal's anonymous reviewers for their constructive comments on earlier versions of
779 this manuscript. The tree-ring data will be made available upon request by Xiaomin
780 Zeng (zengxm1021@suun.edu.cn).
781
782 **Author contributions**

X. Z., M. N. E., and X. L. designed the study. X. Z. performed the analysis and wrote the manuscript with assistance from W. W., G. X., G. W., and L. Z., All authors discussed and commented on the manuscript.

References

Adams, H.D., Guardiola-Claramonte, M., Barron-Gafford, G.A., Villegas, J.C., Breshears, D.D., Zou, C.B., et al., 2009. Temperature sensitivity of drought-induced tree mortality portends increased regional die-off under global-change-type drought. Proceedings of the National Academy of Sciences of the USA 106(17), 7063-7066. https://doi.org/10.1073/pnas.0901438106

Ainsworth, E.A., Long, S.P., 2005. What have we learned from 15 years of free-air CO_2 enrichment (FACE)? A meta-analytic review of the responses of photosynthesis, canopy properties and plant production to rising CO_2. New Phytologist 165(2), 351-372. https://doi.org/10.1111/j.1469-8137.2004.01224.x

Allen, C.D., Macalady, A.K., Chenchouni, H., Bachelet, D., McDowell, N., Vennetier, M., et al., 2010. A global overview of drought and heat-induced tree mortality reveals emerging climate change risks for forests. For. Ecol. Manage. 259(4), 660-684. https://doi.org/10.1016/j.foreco.2009.09.001

Anchukaitis, K.J., Evans, M.N., Kaplan, A., Vaganov, E.A., Hughes, M.K., Grissino-Mayer, H.D., Cane, M.A., 2006. Forward modeling of regional scale

804 tree-ring patterns in the southeastern United States and the recent influence of
805 summer drought. Geophys. Res. Lett. 33(4).
806 https://doi.org/10.1029/2005gl025050
807 Anderegg, W.R.L., Schwalm, C., Biondi, F., Camarero, J.J., Koch, G., Litvak, M., et
808 al., 2015. Pervasive drought legacies in forest ecosystems and their
809 implications for carbon cycle models. Science 349(6247), 528-532.
810 https://doi.org/10.1126/science.aab1833
811 Arend, M., Fromm, J., 2007. Seasonal change in the drought response of wood cell
812 development in poplar. Tree Physiol. 27(7), 985-992.
813 https://doi.org/10.1093/treephys/27.7.985
814 Belien, E., Rossi, S., Morin, H., Deslauriers, A., 2012. Xylogenesis in black spruce
815 subjected to rain exclusion in the field. Can. J. For. Res. 42(7), 1306-1315.
816 https://doi.org/10.1139/x2012-095
817 Breitenmoser, P., Brönnimann, S., Frank, D., 2014. Forward modelling of tree-ring
818 width and comparison with a global network of tree-ring chronologies. Clim.
819 Past. 10(2), 437-449. https://doi.org/10.5194/cp-10-437-2014
820 Brekke, L., Thrasher, B., Maurer, E., Pruitt, T., 2013. Downscaled CMIP3 and
821 CMIP5 Climate and Hydrology Projections: Release of Downscaled CMIP5
822 Climate Projections, Comparison with Preceding Information, and Summary
823 of User Needs. U.S. Dept. of the Interior, Bureau of Reclamation, Technical
824 Services Center, Denver, Colorado.

825 Breshears, D.D., Cobb, N.S., Rich, P.M., Price, K.P., Allen, C.D., Balice, R.G., et al.,
826 2005. Regional vegetation die-off in response to global-change-type drought.
827 Proc. Nat. Acad. Sci. U.S.A. 102(42), 15144-15148.
828 https://doi.org/10.1073/pnas.0505734102
829 Cai, Q., Liu, Y., 2013. Climatic response of Chinese pine and PDSI variability in the
830 middle Taihang Mountains, north China since 1873. Trees 27(2), 419-427.
831 https://doi.org/10.1007/s00468-012-0812-6
832 Cai, Q., Liu, Y., Lei, Y., Bao, G., Sun, B., 2014. Reconstruction of the
833 March–August PDSI since 1703 AD based on tree rings of Chinese pine
834 (*Pinus tabulaeformis* Carr.) in the Lingkong Mountain, southeast Chinese
835 loess Plateau. Clim. Past. 10(2), 509-521.
836 https://doi.org/10.5194/cp-10-509-2014
837 Cai, Q., Liu, Y., Liu, H., Ren, J., 2015. Reconstruction of drought variability in North
838 China and its association with sea surface temperature in the joining area of
839 Asia and Indian–Pacific Ocean. Paleogeogr. Paleoclimatol. Paleoecol. 417,
840 554-560. https://doi.org/10.1016/j.palaeo.2014.10.021
841 Camarero, J.J., Gazol, A., Sancho-Benages, S., Sangüesa-Barreda, G., 2015a. Know
842 your limits? Climate extremes impact the range of Scots pine in unexpected
843 places. Ann. Bot. 116(6), 917-927. https://doi.org/10.1093/aob/mcv124
844 Camarero, J.J., Gazol, A., Sangüesa-Barreda, G., Oliva, J., Vicente-Serrano, S.M.,
845 2015b. To die or not to die: early warnings of tree dieback in response to a

severe drought. J. Ecol. 103(1), 44-57. https://doi.org/10.1111/1365-2745.12295

Chaves, M.M., Maroco, J.P., Pereira, J.S., 2003. Understanding plant responses to drought: from genes to the whole plant. Funct. Plant Biol. 30(3), 239-264. https://doi.org/10.1071/FP02076

Chaves, M.M., Pereira, J.S., Maroco, J., Rodrigues, M.L., Ricardo, C.P.P., Osório, M. L., et al., 2002. How plants cope with water stress in the field? Photosynthesis and growth. Ann. Bot. 89(7), 907-916. https://doi.org/10.1093/aob/mcf105

Chen, L., Huang, J.-G., Ma, Q., Hänninen, H., Tremblay, F., Bergeron, Y., 2019. Long-term changes in the impacts of global warming on leaf phenology of four temperate tree species. Global Change Biol. 25, 997-1004. https://doi.org/10.1111/gcb.14496

Chen, L., Huang, J.-G., Stadt, K.J., Comeau, P.G., Zhai, L., Dawson, A., Alam, S.A., 2017. Drought explains variation in the radial growth of white spruce in western Canada. Agric. For. Meteorol. 233, 133-142. https://doi.org/10.1016/j.agrformet.2016.11.012

Chen, T., de Jeu, R. A.M., Liu, Y.Y., van der Werf, G.R., Dolman, A.J., 2014. Using satellite based soil moisture to quantify the water driven variability in NDVI: a case study over mainland Australia. Remote Sens. Environ. 140, 330-338. https://doi.org/10.1016/j.rse.2013.08.022

Chmielewski, F.-M., Rötzer, T., 2001. Response of tree phenology to climate change across Europe. Agric. For. Meteorol. 108(2), 101-112. https://doi.org/10.1016/S0168-1923(01)00233-7

Collins, M., Knutti, R., Arblaster, J.M., Dufresne, J.-L., Fichefet, T., et. al., 2014. Long-term climate change: projections, commitments and irreversibility, In: T.F. Stocker, D. Qin, G.-K. Plattner, M. Tignor, S.K. Allen, J. Boschung, A. Nauels, Y. Xia, V. Bex, and P.M. Midgley (Eds.), Climate Change 2013: The Physical Science Basis. Cambridge University Press, New York, pp. 1029-1136.

Cook, E.R., 1985. A time series analysis approach to tree-ring standardization. PhD dissertation. University of Arizona, Tucson, AZ, USA.

Cropper, J.P., 1979. Tree-ring skeleton plotting by computer. Tree-ring Bulletin 39, 47–59.

Dai, A., 2013. Increasing drought under global warming in observations and models. Nat. Clim. Chang. 3, 52. https://doi.org/10.1038/nclimate1633

Dai, A., Trenberth, K. E., Qian, T., 2004. A global dataset of Palmer Drought Severity Index for 1870–2002: relationship with soil moisture and effects of surface warming. J. Hydrometeorol. 5(6), 1117-1130. https://doi.org/10.1175/jhm-386.1

D'Arrigo, R.D., Jacoby, G.C., 1991. A 1000-year record of winter precipitation from northwestern New Mexico, USA: a reconstruction from tree-rings and its

887 relation to El Niño and the Southern Oscillation. The Holocene 1(2), 95-101.
888 https://doi.org/10.1177/095968369100100201
889 Evans, M.N., Reichert, B.K., Kaplan, A., Anchukaitis, K.J., Vaganov, E.A., Hughes,
890 M.K., Cane, M.A., 2006. A forward modeling approach to paleoclimatic
891 interpretation of tree-ring data. J. Geophys. Res. G: Biogeosci. 111(G3).
892 https://doi.org/10.1029/2006jg000166
893 Fang, K., Gou, X., Chen, F., Liu, C., Davi, N., Li, J., et al., 2012. Tree-ring based
894 reconstruction of drought variability (1615–2009) in the Kongtong Mountain
895 area, northern China. Global Planet. Change 80-81, 190-197.
896 https://doi.org/10.1016/j.gloplacha.2011.10.009
897 Fritts H.C., 2001. Tree Rings and Climate. Blackburn Press, Caldwell, London.
898 Gao, L., Gou, X., Deng, Y., Wang, Z., Gu, F., Wang, F., 2018. Increased growth of
899 Qinghai spruce in northwestern China during the recent warming hiatus. Agric.
900 For. Meteorol. 260-261, 9-16. https://doi.org/10.1016/j.agrformet.2018.05.025
901 Gao, S., Liu, R., Zhou, T., Fang, W., Yi, C., Lu, R., et al., 2018. Dynamic responses
902 of tree-ring growth to multiple dimensions of drought. Global Change Biol.
903 24(11), 5380-5390. https://doi.org/10.1111/gcb.14367
904 Gonzalez-Benecke, C.A., Teskey, R.O., Dinon-Aldridge, H., Martin, T.A., 2017.
905 *Pinus taeda* forest growth predictions in the 21st century vary with site mean
906 annual temperature and site quality. Global Change Biol. 23(11), 4689-4705.
907 https://doi.org/10.1111/gcb.13717

908 Gou, X., Chen, F., Yang, M., Li, J., Peng, J., Jin, L., 2005. Climatic response of thick
909 leaf spruce (*Picea crassifolia*) tree-ring width at different elevations over
910 Qilian Mountains, northwestern China. J. Arid Environ. 61, 513-524.
911 https://doi.org/10.1016/j.jaridenv.2004.09.011
912 Gou, X., Gao, L., Deng, Y., Chen, F., Yang, M., Still, C., 2015. An 850-year
913 tree-ring-based reconstruction of drought history in the western Qilian
914 Mountains of northwestern China. Int. J. Clim. 35(11), 3308-3319.
915 https://doi.org/10.1002/joc.4208
916 Hagedorn, F., Joseph, J., Peter, M., Luster, J., Pritsch, K., Geppert, U., et al., 2016.
917 Recovery of trees from drought depends on belowground sink control. Nat.
918 Plants 2, 16111. https://doi.org/10.1038/nplants.2016.111
919 He, M., Shishov, V., Kaparova, N., Yang, B., Bräuning, A., Grießinger, J., 2017.
920 Process-based modeling of tree-ring formation and its relationships with
921 climate on the Tibetan Plateau. Dendrochronologia 42, 31-41.
922 https://doi.org/10.1016/j.dendro.2017.01.002
923 Hogg, E.H., 1997. Temporal scaling of moisture and the forest-grassland boundary in
924 western Canada. Agric. For. Meteorol. 84(1), 115-122.
925 https://doi.org/10.1016/S0168-1923(96)02380-5
926 Hogg, E.H., Barr, A.G., Black, T.A., 2013. A simple soil moisture index for
927 representing multi-year drought impacts on aspen productivity in the western

928 Canadian interior. Agricultural and Forest Meteorology 178-179, 173-182.
929 https://doi.org/10.1016/j.agrformet.2013.04.025
930 Holmes, R.L., 1983. Computer-assisted quality control in tree-ring dating and
931 measurement. Tree Ring Bulletin 43, 69–78.
932 Huang, J.P., Guan, X., Ji, F., 2012. Enhanced cold-season warming in semi-arid
933 regions. Atmos. Chem. Phys. 12(12), 5391-5398.
934 https://doi.org/10.5194/acp-12-5391-2012
935 Huang, J.P., Ji, M., Xie, Y., Wang, S., He, Y., Ran, J. 2015a. Global semi-arid climate
936 change over last 60 years. Clim. Dyn. 46(3-4), 1131-1150.
937 https://doi.org/10.1007/s00382-015-2636-8
938 Huang, J., van den Dool, H.M., Georgarakos, K.P., 1996. Analysis of
939 model-calculated soil moisture over the United States (1931–1993) and
940 applications to long-range temperature forecasts. J. Clim. 9(6), 1350-1362.
941 Huang, J. P., Yu, H., Guan, X., Wang, G., Guo, R., 2015b. Accelerated dryland
942 expansion under climate change. Nat. Clim. Chang. 6(2), 166-171.
943 https://doi.org/10.1038/nclimate2837
944 Huete, A., 2016. Vegetation's responses to climate variability. Nature, 531, 181.
945 https://doi.org/10.1038/nature17301
946 Ji, L., Peters, A.J., 2003. Assessing vegetation response to drought in the northern
947 Great Plains using vegetation and drought indices. Remote Sens. Environ.
948 87(1), 85-98. https://doi.org/10.1016/S0034-4257(03)00174-3

949 Karnosky, D.F., 2003. Impacts of elevated atmospheric CO_2 on forest trees and forest
950 ecosystems: knowledge gaps. Environ. Int. 29(2-3), 161-169.
951 https://doi.org/10.1016/s0160-4120(02)00159-9
952 Keenan, T., Maria Serra, J., Lloret, F., Ninyerola, M., Sabate, S., 2011. Predicting the
953 future of forests in the Mediterranean under climate change, with niche- and
954 process-based models: CO_2 matters! Global Change Biol. 17(1), 565-579.
955 https://doi.org/10.1111/j.1365-2486.2010.02254.x
956 Klein, T., Hoch, G., Yakir, D., Körner, C., 2014. Drought stress, growth and
957 nonstructural carbohydrate dynamics of pine trees in a semi-arid forest. Tree
958 physiology 34(9), 981-992. https://doi.org/10.1093/treephys/tpu071
959 Klein, T., Randin, C., Körner, C., 2015. Water availability predicts forest canopy
960 height at the global scale. Ecology letters 18(12), 1311-1320.
961 https://doi.org/10.1111/ele.12525
962 Körner, C., Basler, D., 2010. Phenology under global warming. Science 327(5972),
963 1461-1462. https://doi.org/10.1126/science.1186473
964 Lavergne, A., Daux, V., Villalba, R., Barichivich, J., 2015. Temporal changes in
965 climatic limitation of tree-growth at upper treeline forests: contrasted
966 responses along the west-to-east humidity gradient in northern Patagonia.
967 Dendrochronologia 36, 49-59. https://doi.org/10.1016/j.dendro.2015.09.001
968 Lelieveld, J., Proestos, Y., Hadjinicolaou, P., Tanarhte, M., Tyrlis, E., Zittis, G., 2016.
969 Strongly increasing heat extremes in the Middle East and North Africa

(MENA) in the 21st century. Clim. Change 137(1), 245-260. https://doi.org/10.1007/s10584-016-1665-6

Lévesque, M., Rigling, A., Bugmann, H., Weber, P., Brang, P., 2014. Growth response of five co-occurring conifers to drought across a wide climatic gradient in Central Europe. Agric. For. Meteorol. 197, 1-12. https://doi.org/10.1016/j.agrformet.2014.06.001

Li, G., Harrison, S. P., Prentice, I. C., Falster, D., 2014. Simulation of tree-ring widths with a model for primary production, carbon allocation, and growth. Biogeosciences, 11(23), 6711-6724. https://doi.org/10.5194/bg-11-6711-2014

Li, Q., Yuan, Y.J., Zhang, R.B, Wei, W.S., Yu, S.L., Fan, Z. Shang, H.M., 2016. Tree-ring response to snow cover and reconstruction of century annual maximum snow depth for northern Tianshan Mountains, China. Geochronometria 43(1), 9-17. https://doi.org/10.1515/geochr-2015-0026

Liang, E., Liu, X., Yuan, Y., Qin, N., Fang, X., Huang, L., et al., 2006. The 1920s drought recorded by tree rings and historical documents in the semi-arid and arid areas of Northern China. Clim. Change 79(3-4), 403-432. https://doi.org/10.1007/s10584-006-9082-x

Liang, E., Leuschner, C., Dulamsuren, C., Wagner, B., Hauck, M., 2016. Global warming-related tree growth decline and mortality on the north-eastern Tibetan plateau. Clim. Change 134(1-2), 163-176. https://doi.org/10.1007/s10584-015-1531-y

991 Liu, H., Park Williams, A., Allen, C.D., Guo, D., Wu, X., Anenkhonov, O.A., et al.,
992 2013. Rapid warming accelerates tree growth decline in semi-arid forests of
993 Inner Asia. Global Change Biol. 19(8), 2500-2510.
994 https://doi.org/10.1111/gcb.12217
995 Liu, L., Zhang, Y., Wu, S., Li, S., Qin, D., 2018. Water memory effects and their
996 impacts on global vegetation productivity and resilience. Sci. Rep. 8(1), 2962.
997 https://doi.org/10.1038/s41598-018-21339-4
998 Liu, X., Qin, D., Shao, X., Chen, T., Ren, J., 2005. Temperature variations recorded in
999 tree-rings of middle Qilian Mountains during the last millennium. Science in
1000 China, series D-Earth Sciences 8, 521-529.
1001 Liu, X., Shao, X., Liang, E., Zhao, L., Chen, T., Qin, D., Ren, J., 2007.
1002 Species-dependent responses of juniper and spruce to increasing CO_2
1003 concentration and to climate in semi-arid and arid areas of northwestern China.
1004 Plant Ecol. 193(2), 195. https://doi.org/10.1007/s11258-006-9258-5
1005 Liu, Y., Zhang, X., Song, H., Cai, Q., Li, Q., Zhao, B., et al., 2017.
1006 Tree-ring-width-based PDSI reconstruction for central Inner Mongolia, China
1007 over the past 333 years. Clim. Dyn. 48(3), 867-879.
1008 https://doi.org/10.1007/s00382-016-3115-6
1009 Lotsch, A., Friedl, M. A., Anderson, B. T., Tucker, C. J., 2003. Coupled
1010 vegetation-precipitation variability observed from satellite and climate records.
1011 Geophys. Res. Lett. 30(14). https://doi.org/10.1029/2003GL017506

1012 Lu, C., Wang., L., Xie. G., Leng Y., 2007. Altitude effect of precipitation and spatial
1013 distribution of Qinghai-Tibetan Plateau. J Mt. Sci. 25, 655–663.
1014 McDowell, N., Pockman, W.T., Allen, C.D., Breshears, D.D., Cobb, N., Kolb, T., et
1015 al., 2008. Mechanisms of plant survival and mortality during drought: why do
1016 some plants survive while others succumb to drought? New Phytol. 178(4),
1017 719-739. https://doi.org/10.1111/j.1469-8137.2008.02436.x
1018 McDowell, N.G., Allen, C.D., 2015. Darcy's law predicts widespread forest mortality
1019 under climate warming. Nat. Clim. Chang. 5, 669.
1020 https://doi.org/10.1038/nclimate2641
1021 McMahon, S.M., Parker, G.G., Miller, D.R., 2010. Evidence for a recent increase in
1022 forest growth. Proc. Nat. Acad. Sci. U.S.A. 107(8), 3611-3615.
1023 https://doi.org/10.1073/pnas.0912376107
1024 Mina, M., Martin-Benito, D., Bugmann, H., Cailleret, M., 2016. Forward modeling of
1025 tree-ring width improves simulation of forest growth responses to drought.
1026 Agric. For. Meteorol. 221, 13-33.
1027 https://doi.org/10.1016/j.agrformet.2016.02.005
1028 Misson, L., Rathgeber, C., Guiot, J., 2004. Dendroecological analysis of climatic
1029 effects on *Quercus petraea* and *Pinus halepensis* radial growth using the
1030 process-based MAIDEN model. Can. J. For. Res. 34(4), 888-898.
1031 https://doi.org/10.1139/x03-253

1032 Neuwirth, B., Schweingruber, F. H., Winiger, M., 2007. Spatial patterns of central
1033 European pointer years from 1901 to 1971. Dendrochronologia 24(2-3), 79-89.
1034 https://doi.org/10.1016/j.dendro.2006.05.004
1035 Palmer W.C., 1965. Meteorological Drought. Washington DC: US Department of
1036 Commerce.
1037 Peltier, D.M.P., Barber, J.J., Ogle, K., McGlone, M., 2018. Quantifying antecedent
1038 climatic drivers of tree growth in the Southwestern US. J. Ecol. 106(2),
1039 613-624. https://doi.org/10.1111/1365-2745.12878
1040 Peng, C., Ma, Z., Lei, X., Zhu, Q., Chen, H., Wang, W., et al., 2011. A
1041 drought-induced pervasive increase in tree mortality across Canada's boreal
1042 forests. Nat. Clim. Chang. 1(9), 467-471. https://doi.org/10.1038/nclimate1293
1043 Pinheiro, J.C., Bates, D.M., 2000. Mixed-Effects Models in S and SPLUS. Springer,
1044 New York.
1045 Popkova, M.I., Vaganov, E.A., Shishov, V.V., Babushkina, E.A., Rossi, S., Fonti, M.
1046 V., Fonti, P., 2018. Modeled tracheidograms disclose drought influence on
1047 *Pinus sylvestris* tree-rings structure from Siberian Forest-Steppe. Front. Plant
1048 Sci. 9, 1144. https://doi.org/10.3389/fpls.2018.01144
1049 Poulter, B., Frank, D., Ciais, P., Myneni, R. B., Andela, N., Bi, J., et al., 2014.
1050 Contribution of semi-arid ecosystems to interannual variability of the global
1051 carbon cycle. Nature 509, 600. https://doi.org/10.1038/nature13376

Pretzsch, H., Biber, P., Schütze, G., Uhl, E., Rötzer, T., 2014. Forest stand growth dynamics in Central Europe have accelerated since 1870. Nat. Commun. 5, 4967. https://doi.org/10.1038/ncomms5967

Richard, Y., Martiny, N., Fauchereau, N., Reason, C., Rouault, M., Vigaud, N., Tracol, Y., 2008. Interannual memory effects for spring NDVI in semi-arid South Africa. Geophys. Res. Lett. 35(13). https://doi.org/10.1029/2008GL034119

Sánchez-Salguero, R., Camarero, J.J., Carrer, M., Gutiérrez, E., Alla, A.Q., Andreu-Hayles, L., et al., 2017a. Climate extremes and predicted warming threaten Mediterranean Holocene firs forests refugia. Proc. Nat. Acad. Sci. U.S.A. 114(47), E10142-E10150. https://doi.org/10.1073/pnas.1708109114

Sánchez-Salguero, R., Camarero, J.J., Gutierrez, E., Gonzalez Rouco, F., Gazol, A., Sanguesa-Barreda, G., et al., 2017b. Assessing forest vulnerability to climate warming using a process-based model of tree growth: bad prospects for rear-edges. Global Change Biol. 23(7), 2705-2719. https://doi.org/10.1111/gcb.13541

Salzer, M.W., Hughes, M.K., Bunn, A.G., Kipfmueller, K.F., 2009. Recent unprecedented tree-ring growth in bristlecone pine at the highest elevations and possible causes. Proc. Nat. Acad. Sci. U.S.A. 106(48), 20348-20353. https://doi.org/10.1073/pnas.0903029106

1071 Schweingruber, F.H., Eckstein, D., Serre-Bachet, F., Bräker, O.U., 1990.
1072 Identification, presentation and interpretation of event years and pointer years
1073 in dendrochronology. Dendrochronologia 8, 9-38.
1074 Schwinning, S., Sala, O.E., 2004. Hierarchy of responses to resource pulses in arid
1075 and semi-arid ecosystems. Oecologia 141(2), 211-220.
1076 https://doi.org/10.1007/s00442-004-1520-8
1077 Shen, W., Jenerette, G.D., Hui, D., Scott, R.L., 2016. Precipitation legacy effects on
1078 dryland ecosystem carbon fluxes: direction, magnitude and biogeochemical
1079 carryovers. Biogeosciences 13(2), 425-439.
1080 https://doi.org/10.5194/bg-13-425-2016
1081 Shishov, V.V., Tychkov, I.I., Popkova, M.I., Ilyin, V.A., Bryukhanova, M.V.,
1082 Kirdyanov, A.V., 2016. VS-oscilloscope: a new tool to parameterize tree
1083 radial growthbased on climate conditions. Dendrochronologia 39, 42–50.
1084 https://doi.org/10.1016/j.dendro.2015.10.001
1085 Sidor, C.G., Popa, I., Vlad, R., Cherubini, P., 2015. Different tree-ring responses of
1086 Norway spruce to air temperature across an altitudinal gradient in the Eastern
1087 Carpathians (Romania). Trees-Struct. Funct. 29, 985-997.
1088 https://doi.org/10.1007/s00468-015-1178-3
1089 Tolwinski-Ward, S.E., Anchukaitis, K.J., Evans, M.N., 2013. Bayesian parameter
1090 estimation and interpretation for an intermediate model of tree-ring width.
1091 Clim. Past. 9(4), 1481-1493. https://doi.org/10.5194/cp-9-1481-2013

1092 Tolwinski-Ward, S.E., Evans, M.N., Hughes, M.K., Anchukaitis, K.J., 2011. An
1093 efficient forward model of the climate controls on interannual variation in
1094 tree-ring width. Clim. Dyn. 36(11-12), 2419-2439.
1095 https://doi.org/10.1007/s00382-010-0945-5
1096 Tumajer, J., Altman, J., Štěpánek, P., Treml, V., Doležal, J., Cienciala, E., 2017.
1097 Increasing moisture limitation of Norway spruce in Central Europe revealed
1098 by forward modelling of tree growth in tree-ring network. Agric. For.
1099 Meteorol. 247, 56-64. https://doi.org/10.1016/j.agrformet.2017.07.015
1100 Vaganov E.A., Anchukaitis, K.J., Evans, M.N., 2011. How well understood are the
1101 processes that create dendroclimatic records? A mechanistic model of the
1102 climatic control on conifer tree-ring growth dynamics, in: Hughes, M.K.,
1103 Swetnam, T.W., Diaz H.F. (Eds), Dendroclimatology. Developments in
1104 Paleoenvironmental Research. Springer-Verlag, The Netherlands, pp. 37–75.
1105 Vaganov, E.A., Hughes, M.K., Kirdyanov, A.V., Schweingruber, F.H., Silkin, P.P.,
1106 1999. Influence of snowfall and melt timing on tree growth in subarctic
1107 Eurasia. Nature 400, 149. https://doi.org/10.1038/22087
1108 Vaganov, E.A., Hughes, M.K., Shashkin, A.V., 2006. Growth Dynamics of Conifer
1109 Tree Rings. Springer, Berlin.
1110 Vicente-Serrano, S.M., Gouveia, C., Camarero, J.J., Beguería, S., Trigo, R.,
1111 López-Moreno, J.I., et al., 2013. Response of vegetation to drought time-scales

across global land biomes. Proc. Nat. Acad. Sci. U.S.A. 110(1), 52-57. https://doi.org/10.1073/pnas.1207068110

Wang, L., Chen, W., 2014. A CMIP5 multimodel projection of future temperature, precipitation, and climatological drought in China. Int. J. Clim. 34(6), 2059-2078. https://doi.org/10.1002/joc.3822

Wang, W., Jia, M., Wang, G., Zhu, W., McDowell, N.G., 2017. Rapid warming forces contrasting growth trends of subalpine fir (*Abies fabri*) at higher- and lower-elevations in the eastern Tibetan Plateau. Forest Ecol. Manag. 402, 135-144. https://doi.org/10.1016/j.foreco.2017.07.043

Wang, W., Liu, X., An, W., Xu, G., Zeng, X., 2012. Increased intrinsic water-use efficiency during a period with persistent decreased tree radial growth in northwestern China: causes and implications. Forest Ecol. Manag. 275, 14-22. https://doi.org/10.1016/j.foreco.2012.02.027

Wang, W., Liu, X., Shao, X., Qin, D., Xu, G., Wang, B., et al., 2015. Differential response of Qilian juniper radial growth to climate variations in the middle of Qilian Mountains and the northeastern Qaidam Basin. Clim. Change 133(2), 237-251. https://doi.org/10.1007/s10584-015-1467-2

Waring, R.H., Gao, L., 2016. Recent reduction in the frequency of frost accounts for most of the increased growth of a high elevation spruce forest in northwestern China. Trees 30(4), 1225-1236. https://doi.org/10.1007/s00468-016-1360-2

1132 Williams, P.A., Allen, C.D., Macalady, A.K., Griffin, D., Woodhouse, C.A., Meko, D.
1133 M., et al., 2013. Temperature as a potent driver of regional forest drought
1134 stress and tree mortality. Nat. Clim. Chang. 3(3), 292-297.
1135 https://doi.org/10.1038/nclimate1693
1136 Williams, A.P., Allen, C.D., Millar, C.I., Swetnam, T.W., Michaelsen, J., Still, C.J.,
1137 Leavitt, S.W., 2010. Forest responses to increasing aridity and warmth in the
1138 southwestern United States. Proc. Nat. Acad. Sci. U.S.A. 107(50),
1139 21289-21294. https://doi.org/10.1073/pnas.0914211107
1140 Wu, D., Zhao, X., Liang, S., Zhou, T., Huang, K., Tang, B., Zhao, W. (2015).
1141 Time-lag effects of global vegetation responses to climate change. Global
1142 Change Biol. 21(9), 3520-3531. https://doi.org/10.1111/gcb.12945
1143 Wu, X., Liu, H., Li, X., Ciais, P., Babst, F., Guo, W., et al., 2018. Differentiating
1144 drought legacy effects on vegetation growth over the temperate Northern
1145 Hemisphere. Global Change Biol. 24(1), 504-516.
1146 https://doi.org/10.1111/gcb.13920
1147 Wu, X., Liu, H., Wang, Y., Deng, M., 2013. Prolonged limitation of tree growth due
1148 to warmer spring in semi-arid mountain forests of Tianshan, northwest China.
1149 Environ. Res. Lett. 8(2), 024016.
1150 https://doi.org/10.1088/1748-9326/8/2/024016
1151 Xu, C., Liu, H., Anenkhonov, O.A., Korolyuk, A.Y., Sandanov, D.V., Balsanova,
1152 L.D., et al., 2017. Long-term forest resilience to climate change indicated by

1153 mortality, regeneration, and growth in semiarid southern Siberia. Global
1154 Change Biol. 23(6), 2370-2382. https://doi.org/10.1111/gcb.13582
1155 Yang, B., He, M., Melvin, T.M., Zhao, Y., Briffa, K.R., 2013. Climate control on tree
1156 growth at the upper and lower treelines: a case study in the qilian mountains,
1157 Tibetan Plateau. PLoS One 8, e69065.
1158 https://doi.org/10.1371/journal.pone.0069065
1159 Yang, B., He, M., Shishov, V., Tychkov, I., Vaganov, E., Rossi, S., et al., 2017. New
1160 perspective on spring vegetation phenology and global climate change based
1161 on Tibetan Plateau tree-ring data. Proc. Nat. Acad. Sci. U.S.A. 114(27),
1162 6966-6971. https://doi.org/10.1073/pnas.1616608114
1163 Yang, B., Kang, S., Ljungqvist, F. C., He, M., Zhao, Y., Qin, C., 2014. Drought
1164 variability at the northern fringe of the Asian summer monsoon region over
1165 the past millennia. Clim. Dyn. 43(3), 845-859.
1166 https://doi.org/10.1007/s00382-013-1962-y
1167 Yin, Z.-Y., Shao, X., Qin, N., Liang, E., 2008. Reconstruction of a 1436-year soil
1168 moisture and vegetation water use history based on tree-ring widths from
1169 Qilian junipers in northeastern Qaidam Basin, northwestern China. Int. J. Clim.
1170 28(1), 37-53. https://doi.org/10.1002/joc.1515
1171 Zhang, L., Jiang, Y., Zhao, S., Dong, M., Chen, H. Y. H., Kang, X. 2016. Different
1172 responses of the radial growth of conifer species to increasing temperature
1173 along altitude gradient: *Pinus tabulaeformisin* the Helan Mountains

(Northwestern China). Pol. J. Ecol. 64(4), 509-525. https://doi.org/10.3161/15052249pje2016.64.4.006

Tables

Table 1 Values of Pearson's correlation coefficient (*r*) for the relationships between the observed standardized tree-ring width chronologies and the modeled tree-ring series based on the Bayesian parameter estimation method. The locations of the chronologies are shown in Figure 1. Significance: $^{n.s.}$ not significant, ** $P<0.01$, *** $P<0.001$.

Western region			Eastern region		
Chronology	**Correlation coefficient (*r*)**	**Degrees of freedom *(df)***	**Chronology**	**Correlation coefficient (*r*)**	**Degrees of freedom *(df)***
QF	0.52^{***}	42	XLM	0.58^{***}	48
JG	0.53^{***}	44	THM	0.49^{***}	51
QKD	0.54^{***}	44	MHLH	0.56^{***}	36
KGM	0.52^{***}	44	SYK	0.61^{***}	52
SDLL	0.68^{***}	51	BS	0.62^{***}	52
SDLH	0.65^{***}	51	NHL	0.59^{***}	38
ZMSH	0.70^{***}	51	MHLL	0.62^{***}	36
ZMSL	0.71^{***}	51	HSS	0.75^{***}	44
DYKL	0.54^{***}	51	HSW	0.71^{***}	44
DYKH	0.56^{***}	51	HSE	0.45^{**}	44
QYGH	0.51^{***}	51	BT	0.70^{***}	26
QYGL	0.51^{***}	51	JGB	0.63^{***}	38
DDSL	0.53^{***}	42	HHT	0.61^{***}	32
DDSH	0.61^{***}	51	QL	0.43^{***}	46
XDH	0.43^{***}	44	BYAB	0.67^{***}	52
CLM	0.49^{***}	42	AES	0.48^{***}	52
			MH	0.41^{**}	52

Figure captions

Figure 1 Map showing the locations of the study sites and moisture trends. Colors show the linear rate of change of the annual mean CRU self-calibrated Palmer Drought Severity Index (scPDSI) from 1960 to 2013 throughout the study region (based on data downloaded from https://climexp.knmi.nl/). The red and green colors indicate significant negative (drier) and positive (wetter) trends, respectively, based on the 95% confidence interval.

Figure 2 Box plots for Pearson's correlation coefficient (r) for the relationship between the tree-ring width indices (TRWi) in the western and eastern sub-regions and the climate variables (top panel) and the proportion of the sites in the time series for which we detected a statistically significant ($P < 0.05$) correlation with the climate variables (bottom panel) from May of the previous year (denoted -1 for all months in the previous year) to October of the current year (denoted 0 for all months in the current year), as well as for the period from April to June (AMJ) in the current growing season and from the previous August to the current July (A(-1) – J(0)). (a) TRWi vs. temperature (T), (b) TRWi vs. precipitation (P), (c) TRWi vs. the self-calibrated Palmer drought severity index (scPDSI), (d) TRWi vs. soil moisture (SM), and (e) TRWi vs. the vapor-pressure deficit (VPD). The horizontal dotted lines in the upper panels indicate the 95% confidence interval. Box plots describe the spread of data: median value (bold black horizonal line), upper and lower quartiles (boxes), and the lower and upper extremes (whiskers), beyond which outliers are

plotted as dots.

Figure 3 Comparisons between modeled and actual values of the tree-ring width index (normalized z values) for the (a) western and (b) eastern sub-regions of semi-arid China and (right panels in both figures) the corresponding mean pattern produced by the VS-Lite model for the simulated mean temperature (g_T), soil moisture (g_M), and solar irradiation (g_E) response functions and integrated relative growth rates (G_r) from January to December (right panel). Comparisons of positive and negative pointer years for the modeled mean g_T (top panel) and g_M (bottom panel) in the (c) western and (d) eastern sub-regions. (e) Inter-annual variation of the calculated mean contributions of soil moisture to the modeled tree-ring width indices, and (right panel) the box plots and distribution of the contribution values in the western and eastern sub-regions from 1960 to 2013. Shaded areas represent the mean ± 2SE. In (a), dashed lines represent significant positive trends over time for the observed and modeled TRWi values for the western sub-region ($y = 0.018x - 26.23$, $P < 0.01$ for mean observed TRWi; $y = 0.021x - 41.39$, $P < 0.001$ for mean modeled TRWi) determined by piecewise linear regression. In (e), we also detected a significant positive trend for the inter-annual variation of the contribution of soil moisture to the modeled TRWi in the eastern sub-region ($y = 0.077x - 71.45$, $P = 0.01$), which was determined by piecewise linear regression. The black dotted lines in (c) and (d) represent the average g_T and g_M over the full period (1960 to 2013). Box plots in (e) describe the spread of data: median value (bold black horizonal line), upper and lower quartiles (boxes), and

1271 the lower and upper extremes (whiskers), beyond which outliers are plotted as dots.

1272 **Figure 4** Comparison of the responses of the mean modeled tree-ring width indices
1273 (TRW_i) under different IPCC emission scenarios (RCP 2.6, 4.5, and 8.5) for the
1274 projected period from 2014 to 2100 in the (a) western and (b) eastern sub-regions of
1275 semi-arid of China, and (right panels) the corresponding mean pattern of the VS-Lite
1276 simulated mean temperature (g_T), soil moisture (g_M), and solar irradiation (g_E)
1277 response functions and partial growth rates (G_r) from January to December. The
1278 shaded areas represent the mean ± 2SE. We detected a significant positive trend in the
1279 mean projected TRWi based on the VS-Lite model in the western region in two
1280 scenarios ($y = 0.007x - 15$, $P < 0.05$ for RCP 4.5; $y = 0.011x - 23.14$, $P < 0.01$ for RCP
1281 8.5), determined by piecewise linear regression (dotted green and red lines,
1282 respectively). We also detected a significant positive trend in the mean projected
1283 TRWi based on the VS-lite model in the eastern region in the same scenarios ($y =$
1284 $0.005x - 11.18$, $P < 0.05$ for RCP 4.5; $y = 0.01x - 20.54$, $P < 0.001$ for RCP 8.5),
1285 determined by piecewise linear regression (dotted green and red lines, respectively).

1286

1287

1288